NUMERICAL SIZE ESTIMATES OF INCLUSIONS IN KIRCHHOFF–LOVE ELASTIC PLATES

ANTONIO BILOTTA, ANTONINO MORASSI, EDI ROSSET,
EMILIO TURCO, AND SERGIO VESSELLA

Abstract. The size estimates approach for Kirchhoff–Love elastic plates allows to determine upper and lower bounds of the area of an unknown elastic inclusion by measuring the work developed by applying a couple field on the boundary of the plate. Although the analytical process by which such bounds are determined is of constructive type, it leads to rather pessimistic evaluations. In this paper we show by numerical simulations how to obtain such bounds for practical applications of the method. The computations are developed for a square plate under various boundary loads and for inclusions of different position, shape and stiffness. The sensitivity of the results with respect to the relevant parameters is also analyzed.

How to cite this paper: This paper has been accepted in International Journal of Solids and Structures, 168 (2019) 58–72 and the final publication is available at https://doi.org/10.1016/j.ijsolstr.2019.03.006.

1. Introduction

Diagnostic methods based on non-destructive testing lead to a class of inverse problems of great interest in several fields of mechanical and civil engineering [1]. Their use is of importance to prevent possible failure of a component or structural member and, more generally, to

Key words and phrases. Non-destructive tests; Kirchhoff-Love plates; inclusions; size estimates.

setup a maintenance plan for a mechanical system. Vibrational-based methods are probably the most common class of non-destructive techniques, particularly for applications on large full-scale structures, such as bridges, buildings and dams [2, 3]. However, there are structural systems important in real-life applications in which static tests can be easily arranged and can provide valuable information for diagnostic purposes [4, 5].

In this paper we are concerned with the determination, within an elastic isotropic thin plate, of the possible presence of an inclusion made by different elastic material by static boundary measurements. This inverse problem describes various situations occurring in engineering applications, such as the appearance of diffuse cracking in reinforced concrete plates or corrosion phenomena in metallic plates, which are usually described by local variation of the elastic coefficients of the material in the regions subject to the degradation, see, for instance, [6, 7].

More precisely, if w denotes the transversal displacement of the middle surface Ω of the plate, one wishes to recover a subset $D \subset\subset \Omega$ in the fourth order Kirchhoff–Love equation

$$\operatorname{div}\left(\operatorname{div}\left((\chi_{\Omega\setminus D}\mathbb{P} + \chi_D\widetilde{\mathbb{P}})\nabla^2 w\right)\right) = 0, \quad \text{in } \Omega, \tag{1}$$

from the knowledge of one pair of Cauchy data taken on the boundary $\partial\Omega$ of Ω, on which - under the assumption of $C^{1,1}$ regularity of $\partial\Omega$ - the following two boundary conditions hold [8, 9]:

$$(\mathbb{P}\nabla^2 w)n \cdot n = -\widehat{M}_n, \quad \text{on } \partial\Omega, \tag{2}$$

$$\operatorname{div}\left(\mathbb{P}\nabla^2 w\right) \cdot n + ((\mathbb{P}\nabla^2 w)n \cdot \tau)_{,s} = (\widehat{M}_\tau)_{,s}\,, \quad \text{on } \partial\Omega. \tag{3}$$

Here, $\mathbb{P}$ is the given fourth order plate tensor describing the response of the material in the reference plate, whereas $\widetilde{\mathbb{P}}$ denotes the corresponding tensor for the inclusion D. Our analysis is restricted to a reference plate made by isotropic material (see constitutive equation (42)). Moreover, in the equations above, χ_D is the characteristic function of the set D; n, τ are the unit outer normal and the unit tangent vector to $\partial\Omega$, respectively; $\widehat{M}_\tau$, $\widehat{M}_n$ denote respectively the twisting moment and bending moment applied on $\partial\Omega$.

The inverse problem described above is severely ill-posed. Even the uniqueness issue, that is, whether a single boundary measurement of Neumann $\{\widehat{M}_\tau,\ \widehat{M}_n\}$ and Dirichlet $\{w, w_{,n}\}$ data allows to uniquely determine the unknown inclusion D, is a challenging open problem. In fact, despite the extensive research developed in this field in the last two decades, a general uniqueness result is not yet available even in other contexts arising, for example, in electrical impedance tomography or in linear elasticity, which involve a second order elliptic equation or system, respectively. We refer, among other contributions, to [10] and [11] for an extensive reference list.

Basing on the above considerations, and following a line of research initiated in electric conductivity ([12], [13], [14]) and linear elasticity ([15], [16]), in the last years a relative modest, but realistic, goal has been pursued in the identification of inclusions in elastic plates: to find efficient and stable estimates of the area of the unknown inclusion from a single static experiment. The basic idea relies on comparing the work W, W_0 exerted by applying a given couple field $\widehat{M}$ at the boundary $\partial\Omega$ of the plate in a possibly defected and in the reference state, respectively. When the reference plate is made by isotropic material, and some slight a priori assumptions on the unknown inclusion

are satisfied, the following upper and lower bounds of the area of $|D|$ have been found in [17]:

$$C_1 \left| \frac{W - W_0}{W_0} \right| \leq \text{area(D)} \leq C_2 \left| \frac{W - W_0}{W_0} \right|, \tag{4}$$

where the constants C_1, C_2 only depend on the a priori data. Extensions to Kirchhoff–Love plates whose material belongs to a suitable class of anisotropy are given in [18]. The limit cases of rigid inclusions or cavities require a specific analysis and were considered in [19]. We refer also to [20, 21] for analogous results obtained for shell structures and to [22] for an extension to thick elastic plates described within the Mindlin–Reissner's theory. For the sake of completeness, we recall that an alternative approach to the evaluation of the volume of inclusions has been developed in [23] in the conductivity framework in case of small inclusions and considering multiple boundary measurements.

In our size estimates (4), the area of D is estimated in terms of the normalized work gap $\left|\frac{W-W_0}{W_0}\right|$. It is worth noticing that this quantity can be easily measured in experiments, since both W and W_0 are determined in terms of boundary measurements (see expressions (59) and (60) below). However, the concrete evaluation of the constants C_1, C_2 appearing in (4) is a crucial aspect for concrete applications. In fact, previous studies in electrical conductivity [24] and in two and three-dimensional linear elasticity [25], [26] show that, although the analytical procedure by which such constants are determined is indeed of constructive type, it leads to rather pessimistic estimates. Therefore, it is significant and useful for practical applications to estimate these constants by means of numerical simulations. The present paper is a first contribution to this issue for a Kirchhoff–Love plate.

We have performed an extended series of numerical simulations for a rectangular reference plate made by homogeneous isotropic material and subject to various sets of Neumann data. The configuration considered is rather simple, but it reproduces, among others, the classical bending and torsional tests which are frequently used in quality control of plate specimens. Numerical analysis was based on the implementation of a finite element model based on three-nodes Specht's triangular element [27]. The outcomes of simulations confirm the validity of the theoretical result (4), and show that the points $\left(\left|\frac{W-W_0}{W_0}\right|, |D|\right)$ are located inside an angular sector defined by two straight lines passing through the origin. The comparison between theoretical and numerical estimates of the constants C_1, C_2 appearing in the size estimates (4) and shown in Table 1 further confirms that the analytical process through which such constants are derived leads to highly pessimistic evaluations. Other aspects have been investigated in numerical simulations, such as the effect caused by inclusions stiffer or softer with respect to the background material, and the influence of the minimum distance assumed between D and the boundary of Ω.

Finally, it is important to note that, although very common in applications, the choice of considering a plate with rectangular shape poses additional difficulties in the mathematical formulation of the equilibrium problem due to the presence of corners. It is well known, since the celebrated paper by Lamb [28], that the presence of corners on the boundary of the plate, implies the occurrence of additional conditions which involve point-wise values of second order derivatives up to the boundary. A rigorous mathematical justification of the strong formulation of the Neumann equilibrium problem in this context seems not completely yet available, therefore in our analysis we have assumed

that the transverse deflection w of the plate belongs to the Sobolev space $H^4(\Omega)$. We refer to section 2 for more details on this issue.

The plan of the paper is as follows. In Section 2 we introduce some notation and the variational formulation of the direct problem for a Kirchhoff–Love plate with piecewise-regular boundary. The size estimates results are recalled in Section 3. The results of numerical simulations are reported and discussed in Section 4. Some concluding remarks are collected in Section 5.

2. The direct problem

2.1. **Notation.** Throughout this paper we shall consider a bounded domain Ω in $\mathbb{R}^2$ having Lipschitz boundary $\partial\Omega$ with constants ρ_0, A_0, that is, $\partial\Omega$ is locally the graph of a Lipschitz continuous function with Lipschitz constant A_0 in a disc of radius ρ_0. Moreover, the boundary $\partial\Omega$ is assumed to be a finite union of closed $C^{1,1}$ curves ω_q, $q = 1, ..., Q$, where

$$\omega_q \cap \omega_{q+1} = V_{q+1}, \tag{5}$$

with $\omega_{Q+1} = \omega_1$, $V_{Q+1} = V_1$.

For any q, $q = 1, ..., Q$, let us define as positive the orientation of ω_q associated to the arclength parametrization $\varphi(s) = (x_1(s), x_2(s))$, $s \in [0, \ell(\omega_q)]$, such that $\varphi(0) = V_q$ and $\varphi'(s) = \tau(\varphi(s))$. Here, $\ell(\omega_q)$ denotes the length of ω_q, and τ is the unit tangent at ω_q given by

$$\tau = e_3 \times n, \tag{6}$$

where n is the unit outer normal to $\partial\Omega$, $\times$ denotes the vector product in $\mathbb{R}^3$, and $\{e_1, e_2, e_3\}$ is the canonical basis in $\mathbb{R}^3$.

We shall refer to a plane domain Ω satisfying all the above properties as a *piecewise-regular* domain with constants ρ_0, A_0.

We denote by $w_{,\alpha}$, $w_{,s}$, $w_{,n}$ the derivatives of a function w with respect to the x_α variable, to the arclength s, and to the normal direction n, respectively, and similarly for higher order derivatives.

For every 2×2 matrices A, B and for every $\mathbb{L} \in \mathcal{L}(\mathbb{M}^2, \mathbb{M}^2)$, we adopt the standard notation

$$(\mathbb{L}A)_{\alpha\beta} = L_{\alpha\beta\gamma\delta} A_{\gamma\delta}, \tag{7}$$

$$A \cdot B = A_{\alpha\beta} B_{\alpha\beta}, \tag{8}$$

$$|A| = (A \cdot A)^{\frac{1}{2}}, \tag{9}$$

$$A^{sym} = \frac{1}{2}\left(A + A^T\right), \tag{10}$$

where A^T is the transpose matrix of A and summation over repeated indexes is implied. Moreover, given $\mathbb{L}$, $\widetilde{\mathbb{L}} \in \mathcal{L}(\mathbb{M}^2, \mathbb{M}^2)$, we shall say that $\widetilde{\mathbb{L}} \leq \mathbb{L}$ if and only if

$$\widetilde{\mathbb{L}}A \cdot A \leq \mathbb{L}A \cdot A \tag{11}$$

for every 2×2 symmetric matrix A.

The norms of all the functions defined either in Ω or on $\partial\Omega$ are normalized such that their terms are dimensionally homogeneous with the argument of the norm and coincide with the standard definition when $\rho_0 = 1$.

2.2. **Variational formulation of the direct problem.** Let $\Omega \times \left[-\frac{h}{2}, \frac{h}{2}\right]$ be a thin elastic plate, whose middle surface Ω is a *piecewise-regular* domain with constants ρ_0, A_0. We shall also assume that, for some positive constant A_1,

$$|\Omega| \leq A_1 \rho_0^2. \tag{12}$$

The plate is made of nonhomogeneous linearly elastic material, with elastic tensor $\mathbb{C}(x) \in \mathcal{L}(\mathbb{M}^2, \mathbb{M}^2)$, and body forces inside Ω are absent. On the tensor $\mathbb{C}$, we assume:

i) *Regularity*:

$$\mathbb{C} \in L^\infty(\Omega, \mathcal{L}(\mathbb{M}^2, \mathbb{M}^2)); \tag{13}$$

ii) *Symmetry conditions*:

$$C_{\alpha\beta\gamma\delta} = C_{\gamma\delta\alpha\beta} = C_{\gamma\delta\beta\alpha} \quad \alpha, \beta, \gamma, \delta = 1, 2, \text{ a.e. in } \Omega, \tag{14}$$

where $C_{\alpha\beta\gamma\delta}$ are the cartesian components of the elasticity tensor $\mathbb{C}$;

iii) *Strong convexity*:

$$\mathbb{C}A \cdot A \geq \xi_0 |A|^2, \qquad \text{a.e. in } \Omega, \tag{15}$$

for every 2×2 symmetric matrix A and for some positive constant ξ_0.

The *plate tensor* $\mathbb{P} = \mathbb{P}(x)$ is defined by

$$\mathbb{P} = \frac{h^3}{12}\mathbb{C}. \tag{16}$$

Let

$$\widehat{\mathbf{M}} = (\widehat{M}_2, \widehat{M}_1) \in H^{-\frac{1}{2}}(\partial\Omega, \mathbb{R}^2) \tag{17}$$

be a couple field acting on the boundary, satisfying the compatibility conditions

$$\int_{\partial\Omega} \widehat{M}_\alpha = 0, \qquad \alpha = 1, 2. \tag{18}$$

The energy functional associated to the deformation of the plate under the action of the boundary couple field $\widehat{\mathbf{M}}$ is given by

$$J : H^2(\Omega) \to \mathbb{R}, \qquad J(v) = \frac{1}{2}a(v, v) - l(v), \tag{19}$$

where

$$a(v, u) : H^2(\Omega) \times H^2(\Omega) \to \mathbb{R}, \qquad a(v, u) = \int_\Omega \mathbb{P}\nabla^2 v \cdot \nabla^2 u, \tag{20}$$

$$l(v) : H^2(\Omega) \to \mathbb{R}, \qquad l(v) = \int_{\partial\Omega} \widehat{M}_2 v_{,2} - \widehat{M}_1 v_{,1}\,. \tag{21}$$

The transversal displacement $w = w(x_1, x_2)$ of the middle surface of the plate Ω, induced by the application of the couple field $\widehat{\mathbf{M}}$ at the boundary, is a minimizer of the energy functional J, which attains a unique minimum up to addition of an affine function of the variables x_1, x_2, see, for instance, [17] (Proposition 3.4). In order to univocally determine w, we impose the following normalization conditions

$$\int_\Omega w = 0, \qquad \int_\Omega w_{,\alpha} = 0, \qquad \alpha = 1, 2, \tag{22}$$

under which we have

$$\|w\|_{H^2(\Omega)} \leq C\rho_0^2 \|\widehat{\mathbf{M}}\|_{H^{-\frac{1}{2}}(\partial\Omega,\mathbb{R}^2)}, \tag{23}$$

where $C > 0$ only depends on h, A_0, A_1 and ξ_0.

The strong formulation of the equilibrium problem for a plate with corners is a very delicate matter. The boundary conditions for the Neumann problem are usually derived in mechanical literature (see for instance [29]) assuming a priori further regularity of the solution. On the other hand, Grisvard and Nazaret pointed out delicate aspects of this theory in [30] and [31].

In order to give an idea of the arguments which lead to the derivation of the Neumann boundary conditions, let us assume here that $w \in H^4(\Omega)$.

The first variation of the energy functional J at the solution w is given, for every $h \in H^2(\Omega)$, by

$$\delta J(w)[h] = -\int_\Omega M_{\alpha\beta}(w) h_{,\alpha\beta} - \int_{\partial\Omega} (-\widehat{M}_1 h_{,1} + \widehat{M}_2 h_{,2}\,), \tag{24}$$

where the 2×2 matrix M of the contact couples $(M_{\alpha\beta})$, $\alpha, \beta = 1, 2$, is given by

$$M = -\mathbb{P}\nabla^2 w. \tag{25}$$

Integrating by parts in (24) and noticing that, in local coordinates,

$$h_{,\alpha} = n_\alpha h_{,n} + \tau_\alpha h_{,s}\,, \qquad \text{in } \partial\Omega \setminus \cup_{i=1}^{Q} V_i, \tag{26}$$

we have

$$\begin{aligned} &- \int_\Omega M_{\alpha\beta,\alpha\beta}\,(w)h + \int_{\partial\Omega} M_{\alpha\beta,\beta}\,(w)n_\alpha h - \\ &- \int_{\partial\Omega} h_{,n}\,(M_{\alpha\beta}(w)n_\alpha n_\beta - \widehat{M}_n) - \int_{\partial\Omega} h_{,s}\,(M_{\alpha\beta}(w)n_\beta\tau_\alpha + \widehat{M}_\tau) = 0, \end{aligned} \tag{27}$$

for every $h \in H^2(\Omega)$, where the *bending moment* $\widehat{M}_n$ and the *twisting moment* $\widehat{M}_\tau$ are given by

$$\widehat{M}_n = \widehat{M}_1 n_1 - \widehat{M}_2 n_2, \quad \widehat{M}_\tau = \widehat{M}_1 n_2 + \widehat{M}_2 n_1. \tag{28}$$

By integrating by parts the last integral in (27), we have

$$\begin{aligned} &\int_{\partial\Omega} h_{,s}\,(M_{\alpha\beta}(w)n_\beta\tau_\alpha + \widehat{M}_\tau) = \\ &= \sum_{q=1}^{Q} \int_{\omega_q} \Big(h(M_{\alpha\beta}(w)n_\beta\tau_\alpha + \widehat{M}_\tau)\Big)_{,s} - \sum_{q=1}^{Q} \int_{\omega_q} h(M_{\alpha\beta}(w)n_\beta\tau_\alpha + \widehat{M}_\tau)_{,s}\ . \end{aligned} \tag{29}$$

Now, let us evaluate

$$I(\omega_q) = \int_{\omega_q} \Big(h(M_{\alpha\beta}(w)n_\beta\tau_\alpha + \widehat{M}_\tau)\Big)_{,s}\ . \tag{30}$$

Given a point P_q interior to the curve ω_q, let us split ω_q as the union of the subarcs $\omega_{q,1}$, $\omega_{q,2}$, having end points V_q, P_q and P_q, V_{q+1}, respectively. For any sufficiently small $\epsilon > 0$, let $P_q^\epsilon = \varphi(\epsilon) \in \omega_{q,1}$,

$P^{\epsilon}_{q+1} = \varphi(\ell(\omega_q) - \epsilon) \in \omega_{q,2}$, and let $\omega^{\epsilon}_{q,1}$ and $\omega^{\epsilon}_{q,2}$ be the subarcs of ω_q having end points P^{ϵ}_q, P_q and P_q, P^{ϵ}_{q+1}, respectively.

We have that

$$I(\omega_q) = I(\omega_{q,1}) + I(\omega_{q,2}). \tag{31}$$

Let us consider, for example, $I(\omega_{q,1})$. Since $w \in H^4(\Omega)$, $M_{\alpha\beta}w \in H^{\frac{3}{2}}(\omega_q) \subset W^{1,1}(\omega_q)$, so that $h(M_{\alpha\beta}(w)n_\beta\tau_\alpha + \widehat{M}_\tau)$ is an absolutely continuous function and we may write

$$I(\omega^{\epsilon}_{q,1}) = \left(h(M_{\alpha\beta}(w)n_\beta\tau_\alpha + \widehat{M}_\tau)\right)(P_q) - \left(h(M_{\alpha\beta}(w)n_\beta\tau_\alpha + \widehat{M}_\tau)\right)(P^{\epsilon}_q)$$

Since the function $h\left(M_{\alpha\beta}(w)n_\beta\tau_\alpha + \widehat{M}_\tau)\right)_{,s}$ is integrable over $\omega_{q,1}$, there exists $\lim_{\epsilon\to 0} I(\omega^{\epsilon}_{q,1}) = I(\omega_{q,1})$. Therefore there exists also

$$\left(h(M_{\alpha\beta}(w)n_\beta\tau_\alpha + \widehat{M}_\tau)\right)(V^+_q) \equiv \lim_{\epsilon\to 0}\left(h(M_{\alpha\beta}(w)n_\beta\tau_\alpha + \widehat{M}_\tau)\right)(P^{\epsilon}_q) = \\ = \left(h(M_{\alpha\beta}(w)n_\beta\tau_\alpha + \widehat{M}_\tau)\right)(V_q) - I(\omega_{q,1}). \tag{32}$$

By applying the same arguments to $\omega_{q,2}$, and summing up over $q = 1, ..., Q$, expression (29) becomes

$$\int_{\partial\Omega} h_{,s}\,(M_{\alpha\beta}(w)n_\beta\tau_\alpha + \widehat{M}_\tau) = \\ = \sum_{q=1}^{Q}\left(h(M_{\alpha\beta}(w)n_\beta\tau_\alpha + \widehat{M}_\tau)\right)|^{V^-_{q+1}}_{V^+_q} - \int_{\partial\Omega\setminus\cup_{q=1}^{Q}V_q} h(M_{\alpha\beta}(w)n_\beta\tau_\alpha + \widehat{M}_\tau)_{,s}\ . \tag{33}$$

By the arbitrariness of the test function h, $h \in H^2(\Omega)$, by inserting (33) in (27), we obtain the strong formulation of the equilibrium problem

$$M_{\alpha\beta,\alpha\beta}(w) = 0, \qquad \text{in } \Omega, \tag{34}$$

$$M_{\alpha\beta}(w)n_\alpha n_\beta = \widehat{M}_n, \qquad \text{on } \partial\Omega, \tag{35}$$

$$M_{\alpha\beta,\beta}(w)n_\alpha + (M_{\alpha\beta}(w)n_\beta\tau_\alpha)_{,s} = -(\widehat{M}_\tau)_{,s}\,, \qquad \text{on } \partial\Omega \setminus \cup_{q=1}^{Q}V_q, \tag{36}$$

$$[\![M_{\alpha\beta}(w)n_\beta\tau_\alpha + \widehat{M_\tau}]\!](V_q) = 0, \qquad q = 1, ..., Q, \tag{37}$$

where, for any function f, $f : \partial\Omega \to \mathbb{R}$, the jump of f at a point $V_q \in \partial\Omega$ is denoted by $[\![f]\!](V_q)$.

By recalling (25), the equilibrium problem (34)–(37) for the plate with corners can be rewritten in a compact form as

$$\operatorname{div}(\operatorname{div}(\mathbb{P}\nabla^2 w)) = 0, \quad \text{in } \Omega, \tag{38}$$

$$(\mathbb{P}\nabla^2 w)n \cdot n = -\widehat{M_n}, \quad \text{on } \partial\Omega, \tag{39}$$

$$\operatorname{div}(\mathbb{P}\nabla^2 w) \cdot n + ((\mathbb{P}\nabla^2 w)n \cdot \tau)_{,s} = (\widehat{M_\tau})_{,s}\,, \quad \text{on } \partial\Omega \setminus \cup_{q=1}^{Q} V_q, \tag{40}$$

$$[\![(\mathbb{P}\nabla^2 w)n \cdot \tau - \widehat{M_\tau}]\!](V_q) = 0, \quad q = 1, ..., Q. \tag{41}$$

Let us notice that, once we are able to produce a function $w \in H^4(\Omega)$ which satisfies (34)–(37) in the strong sense, then we can retrace backwards the steps described above, obtaining that w is a weak variational solution to the equilibrium problem, and therefore is determined up to the addition of an affine function. In our test problems (see Section 4), this regularity condition is indeed satisfied.

3. The inverse problem

Let us assume that the plate contains a possible inclusion $D \times \left[-\frac{h}{2}, \frac{h}{2}\right]$, where D is a measurable subset of Ω.

We consider the case when the *background material* is of Lamé type, with plate tensor $\mathbb{P} \in L^\infty(\Omega, \mathcal{L}(\mathbb{M}^2, \mathbb{M}^2))$ defined by

$$\mathbb{P}A = B\left[(1-\nu)A^{sym} + \nu(trA)I_2\right], \tag{42}$$

for every 2×2 matrix A, where I_2 is the 2×2 identity matrix and $\operatorname{tr}(A)$ denotes the trace of A. Here, as standard notation, B is the *bending*

stiffness of the plate,

$$B(x) = \frac{h^3}{12}\left(\frac{E(x)}{1-\nu^2(x)}\right), \tag{43}$$

where the Young's modulus E and the Poisson's coefficient ν are given in terms of the Lamé moduli as

$$E(x) = \frac{\mu(x)(2\mu(x)+3\lambda(x))}{\mu(x)+\lambda(x)}, \qquad \nu(x) = \frac{\lambda(x)}{2(\mu(x)+\lambda(x))}. \tag{44}$$

In this case, the strong convexity condition (15) becomes

$$\mu(x) \geq \alpha_0 > 0, \qquad 2\mu(x)+3\lambda(x) \geq \gamma_0 > 0, \qquad \text{a.e. in } \Omega\,, \tag{45}$$

and, in terms of the Young's modulus E and the Poisson's ratio ν, it becomes

$$E(x) > 0\,, \qquad -1 < \nu(x) < \frac{1}{2}\,, \qquad \text{a.e. in } \Omega\,. \tag{46}$$

We further assume that $\mathbb{P}$ is of $C^{1,1}$ class, that is, there exists $A_2 > 0$ such that

$$\|\lambda\|_{C^{1,1}(\overline{\Omega})} + \|\mu\|_{C^{1,1}(\overline{\Omega})} \leq A_2. \tag{47}$$

The plate tensor inside the inclusion is denoted by $\widetilde{\mathbb{P}}$, $\widetilde{\mathbb{P}} = \frac{h^3}{12}\widetilde{\mathbb{C}}$, where $\widetilde{\mathbb{C}}$ satisfies conditions (13)–(15), The material of the inclusion might be either stiffer or softer than the background material, and we require the following jump conditions:
Either there exist $\eta > 0$ and $\delta > 1$ such that

$$\eta\mathbb{P} \leq \widetilde{\mathbb{P}} - \mathbb{P} \leq (\delta-1)\mathbb{P}, \quad \text{a.e. in } D, \quad (\textit{stiff inclusion}), \tag{48}$$

or there exist $\eta > 0$ and $0 < \delta < 1$ such that

$$\eta\mathbb{P} \leq \mathbb{P} - \widetilde{\mathbb{P}} \leq (1-\delta)\mathbb{P}, \quad \text{a.e. in } D, \quad (\textit{soft inclusion}). \tag{49}$$

Let us consider the plate problem with or without inclusion:

$$\operatorname{div}\left(\operatorname{div}\left((\chi_{\Omega\setminus D}\mathbb{P} + \chi_D\widetilde{\mathbb{P}})\nabla^2 w\right)\right) = 0, \quad \text{in } \Omega, \tag{50}$$

$$(\mathbb{P}\nabla^2 w)n\cdot n = -\widehat{M}_n, \quad \text{on } \partial\Omega, \tag{51}$$

$$\operatorname{div}(\mathbb{P}\nabla^2 w)\cdot n + ((\mathbb{P}\nabla^2 w)n\cdot\tau)_{,s} = (\widehat{M}_\tau)_{,s}\,, \quad \text{on } \partial\Omega\setminus\cup_{q=1}^{Q} V_q, \tag{52}$$

$$[\![(\mathbb{P}\nabla^2 w)n\cdot\tau - \widehat{M}_\tau]\!](V_q) = 0, \quad q = 1, ..., Q, \tag{53}$$

and

$$\operatorname{div}(\operatorname{div}(\mathbb{P}\nabla^2 w_0)) = 0, \quad \text{in } \Omega, \tag{54}$$

$$(\mathbb{P}\nabla^2 w_0)n\cdot n = -\widehat{M}_n, \quad \text{on } \partial\Omega, \tag{55}$$

$$\operatorname{div}(\mathbb{P}\nabla^2 w_0)\cdot n + ((\mathbb{P}\nabla^2 w_0)n\cdot\tau)_{,s} = (\widehat{M}_\tau)_{,s}\,, \quad \text{on } \partial\Omega\setminus\cup_{q=1}^{Q} V_q, \tag{56}$$

$$[\![(\mathbb{P}\nabla^2 w_0)n\cdot\tau - \widehat{M}_\tau]\!](V_q) = 0, \quad q = 1, ..., Q. \tag{57}$$

The solutions w and w_0 are uniquely determined by imposing the normalization conditions (22).

Our size estimates are given in terms of the *normalized work gap*

$$\left|\frac{W - W_0}{W_0}\right|, \tag{58}$$

where

$$W = -\int_{\partial\Omega} \widehat{M}_{\tau,s} w + \widehat{M}_n w_{,n} = \int_\Omega (\chi_{\Omega\setminus D}\mathbb{P} + \chi_D\widetilde{\mathbb{P}})\nabla^2 w\cdot\nabla^2 w, \tag{59}$$

$$W_0 = -\int_{\partial\Omega} \widehat{M}_{\tau,s} w_0 + \widehat{M}_n w_{0,n} = \int_\Omega \mathbb{P}\nabla^2 w_0\cdot\nabla^2 w_0. \tag{60}$$

The analytical bounds of the area of D are stated in [17, Theorem 4.1].

Theorem 3.1. *Under the above assumptions, let D be a measurable subset of Ω satisfying*

$$dist(D, \partial\Omega) \geq d_0\rho_0 \tag{61}$$

and

$$area\,(\{x\in D|\ dist\{x, \partial D\} > h_1\}) \geq \frac{1}{2} area(D) \tag{62}$$

for given positive constants d_0, h_1.

If (48) *holds then we have*

$$\frac{1}{\delta-1}C_1^+\rho_0^2\frac{W_0-W}{W_0}\leq|D|\leq\frac{\delta}{\eta}C_2^+\rho_0^2\frac{W_0-W}{W_0}. \tag{63}$$

If, conversely, (49) *holds then we have*

$$\frac{\delta}{1-\delta}C_1^-\rho_0^2\frac{W-W_0}{W_0}\leq|D|\leq\frac{1}{\eta}C_2^-\rho_0^2\frac{W-W_0}{W_0}, \tag{64}$$

where C_1^+, C_1^- *only depend on* A_0, A_1, d_0, α_0, γ_0, A_2 *and* C_2^+, C_2^- *only depend on the same quantities and, in addition, on* h_1 *and on the ratio of norms* $\frac{\|\widehat{M}\|_{L^2(\partial\Omega)}}{\|\widehat{M}\|_{H^{-\frac{1}{2}}(\partial\Omega)}}$.

The proof of this theorem is mainly based on two steps. In the first one it is shown that $\int_D|\nabla^2w_0|^2$ is comparable to $|W-W_0|$. More precisely, we have the following proposition, see [17, Lemma 5.1].

Proposition 3.2. *Under the above assumptions, if* (48) *holds, then*

$$\frac{\eta\xi_0}{\delta}\int_D|\nabla^2w_0|^2\leq W_0-W\leq(\delta-1)\xi_1\int_D|\nabla^2w_0|^2; \tag{65}$$

if, instead, (49) *holds, then*

$$\eta\xi_0\int_D|\nabla^2w_0|^2\leq W-W_0\leq\frac{1-\delta}{\delta}\xi_1\int_D|\nabla^2w_0|^2, \tag{66}$$

where $\xi_0=\frac{h^3}{12}\min\{2\alpha_0,\gamma_0\}$, $\xi_1=\frac{h^3E}{12(1-\nu^2)}\max\{1-\nu,1+\nu\}$.

The second step consists in controlling the integral $\int_D|\nabla^2w_0|^2$ in terms of the measure of D. In particular, the more difficult aspect consists in estimating from below $\int_D|\nabla^2w_0|^2$, and this task involves refined quantitative estimates of unique continuation for the reference solution w_0, see [17] for details.

4. Numerical simulations

In this section we present and discuss the results of a series of numerical simulations aimed to the evaluation of the constants appearing in Theorem 3.1. We restrict our attention to some model problems, significant for applications, in which explicit expressions of $\nabla^2 w_0$ are available. For these cases, we compare the theoretical prediction with the results of the corresponding numerical simulation.

4.1. **Test problems.** In our numerical experiments we consider a Kirchhoff–Love square plate, with side $a = 0.25$ m and thickness $h = 0.005$ m. The Lamé parameters of the material are $\lambda = 118846$ MPa and $\mu = 79231$ MPa, typical of a mild steel ($\nu = 0,3$). The inclusion is a connected subset of Ω and is made of Lamé material, with plate tensor

$$\widetilde{\mathbb{P}} = f\mathbb{P}, \tag{67}$$

where $f > 0$ is the *stiffness ratio*. All the simulations refer to $\widehat{M} = 500$ Pa. Under this choice of the parameters, we have $\xi_0 = B(1-\nu)$, $\xi_1 = B(1+\nu)$.

We first consider three cases in which the Hessian matrix $\nabla^2 w_0$ does not vanish in Ω. They correspond to the following Neumann boundary conditions: i) bending moments along all the edges; ii) bending moments along two opposite edges; iii) torsional moments along two opposite edges, see Figs. 5(a), 10(a) and 14(a).

i) Bending moments along all the edges:

$$\begin{aligned} &\text{on } x_2 = 0, \quad \widehat{\mathbf{M}} = -\widehat{M}e_1, \quad \text{on } x_2 = a, \quad \widehat{\mathbf{M}} = \widehat{M}e_1, \\ &\text{on } x_1 = 0, \quad \widehat{\mathbf{M}} = \widehat{M}e_2, \qquad \text{on } x_1 = a, \quad \widehat{\mathbf{M}} = -\widehat{M}e_2. \end{aligned}$$

By using the strong formulation (54)–(57), we obtain the Hessian matrix of the solution w_0 in $[0,a]\times[0,a]$:

$$\nabla^2 w_0 = \frac{\widehat{M}}{B(1+\nu)} \begin{vmatrix} 1 & 0 \\ 0 & 1 \end{vmatrix}. \tag{68}$$

ii) Bending moments along two opposite edges:

$$\begin{aligned} &\text{on } x_2=0, \quad \widehat{\mathbf{M}}=0, && \text{on } x_2=a, \quad \widehat{\mathbf{M}}=0,\\ &\text{on } x_1=0, \quad \widehat{\mathbf{M}}=\widehat{M}e_2, && \text{on } x_1=a, \quad \widehat{\mathbf{M}}=-\widehat{M}e_2, \end{aligned}$$

$$\nabla^2 w_0 = \frac{\widehat{M}}{B(1-\nu^2)} \begin{vmatrix} 1 & 0 \\ 0 & -\nu \end{vmatrix}. \tag{69}$$

iii) Torsional moments along two opposite edges:

$$\begin{aligned} &\text{on } x_2=0, \quad \widehat{\mathbf{M}}=0, && \text{on } x_2=a, \quad \widehat{\mathbf{M}}=0,\\ &\text{on } x_1=0, \quad \widehat{\mathbf{M}}=-\widehat{M}e_1, && \text{on } x_1=a, \quad \widehat{\mathbf{M}}=\widehat{M}e_1, \end{aligned}$$

$$\nabla^2 w_0 = \frac{\widehat{M}}{2B(1-\nu)} \begin{vmatrix} 0 & 1 \\ 1 & 0 \end{vmatrix}. \tag{70}$$

Let us notice that $\delta = f$, $\eta = |f-1|$, $\int_D |\nabla^2 w_0|^2 = |D||\nabla^2 w_0|^2$, and computing

$$W_0 = \frac{Eh^3}{12(1-\nu^2)} \left((1-\nu)|\nabla^2 w_0|^2 + \nu(tr(\nabla^2 w_0))^2\right)|\Omega|,$$

we can apply Proposition 3.2 obtaining, in the case of stiff inclusion (see (48))

$$\begin{aligned} \left[\frac{(1-\nu)|\nabla^2 w_0|^2 + \nu(tr(\nabla^2 w_0))^2}{(f-1)(1+\nu)|\nabla^2 w_0|^2}\right]\frac{W_0-W}{W_0} \le \frac{|D|}{|\Omega|} \le \\ \le \left[\frac{f\left((1-\nu)|\nabla^2 w_0|^2 + \nu(tr(\nabla^2 w_0))^2\right)}{(f-1)(1-\nu)|\nabla^2 w_0|^2}\right]\frac{W_0-W}{W_0}, \end{aligned} \tag{71}$$

and

$$\left[\frac{f\left((1-\nu)|\nabla^2 w_0|^2+\nu(tr(\nabla^2 w_0))^2\right)}{(1-f)(1+\nu)|\nabla^2 w_0|^2}\right]\frac{W-W_0}{W_0}\leq\frac{|D|}{|\Omega|}\leq$$
$$\leq\left[\frac{(1-\nu)|\nabla^2 w_0|^2+\nu(tr(\nabla^2 w_0))^2}{(1-f)(1-\nu)|\nabla^2 w_0|^2}\right]\frac{W-W_0}{W_0} \quad (72)$$

for soft inclusion (see (49)).

The non-vanishing of the Hessian matrix can be a restrictive assumption in practical applications. For this reason, it is worthwhile to investigate cases in which this condition is not satisfied. Therefore, let us consider the function $w(x_1,x_2)=\left(x_1-\frac{a}{2}\right)^3$ which solves equation (54) in $[0,a]\times[0,a]$, for any homogeneous isotropic material and whose Hessian matrix vanishes along the line $x_1=\frac{a}{2}$. More precisely,

iv) Hessian vanishing along $x_1=\frac{a}{2}$*:*

$$\begin{aligned}
&\text{on } x_2=0, \quad \widehat{\mathbf{M}}=-B\nu(6x_1-3a)e_1,\\
&\text{on } x_2=a, \quad \widehat{\mathbf{M}}=B\nu(6x_1-3a)e_1+6Bae_2,\\
&\text{on } x_1=0, \quad \widehat{\mathbf{M}}=-6Bx_2e_1-3aBe_2,\\
&\text{on } x_1=a, \quad \widehat{\mathbf{M}}=6Bx_2e_1-3aBe_2.
\end{aligned} \quad (73)$$

$$\nabla^2 w_0=\begin{vmatrix} 6\left(x_1-\frac{a}{2}\right) & 0\\ 0 & 0\end{vmatrix}. \quad (74)$$

We can compute

$$W_0=\frac{h^3E}{12(1-\nu^2)}\int_\Omega|\nabla^2 w_0|^2=\frac{h^3E}{4(1-\nu^2)}a^2|\Omega|, \quad (75)$$

$$\int_D|\nabla^2 w_0|^2\leq 9a^2|D|. \quad (76)$$

From Proposition 3.2, (75) and (76), we have the following lower bounds for the relative measure of stiff inclusions

$$\frac{|D|}{|\Omega|}\geq\left(\frac{1}{3(f-1)(1+\nu)}\right)\frac{W_0-W}{W_0}, \quad (77)$$

and soft inclusions

$$\frac{|D|}{|\Omega|} \geq \left(\frac{f}{3(1-f)(1+\nu)}\right) \frac{W - W_0}{W_0}, \tag{78}$$

respectively.

In order to obtain an upper bound for $\frac{|D|}{|\Omega|}$, and in absence of a positive pointwise lower bound of $|\nabla^2 w_0|$, we look for an integral lower bound. Keeping fixed the area of the inclusion D, the minimum of $\int_D |\nabla^2 w_0|^2$ is reached for the rectangle $D^* = \left[\frac{a}{2} - \gamma, \frac{a}{2} + \gamma\right] \times [0, a]$, where $|D| = 2a\gamma$. A trivial computation gives

$$\int_D |\nabla^2 w_0|^2 \geq 3\frac{|D|^3}{|\Omega|}. \tag{79}$$

Therefore, from Proposition 3.2, (75) and (79), we have the following upper bounds for the relative measure of stiff inclusions

$$\frac{|D|}{|\Omega|} \leq \left(\frac{f}{(f-1)(1-\nu)}\right)^{\frac{1}{3}} \left(\frac{W_0 - W}{W_0}\right)^{\frac{1}{3}}, \tag{80}$$

and soft inclusions

$$\frac{|D|}{|\Omega|} \leq \left(\frac{1}{(1-f)(1-\nu)}\right)^{\frac{1}{3}} \left(\frac{W - W_0}{W_0}\right)^{\frac{1}{3}}, \tag{81}$$

respectively. These estimates are a numerical confirmation of the optimality of the Hölder character of the size estimates from above, which were obtained in an abstract setting in [32, Theorem 3.1]

In fact, in our simulations, we consider inclusions which belong to specific discrete families: they are either squares obtained as union of elementary squares of side $\frac{a}{26}$ or more general sets obtained as union of the triangles described in Figure 2, which have *cathetus* of length $\frac{a}{18}$. Standard computations show that the minimum of $\int_D |\nabla^2 w_0|^2$ is reached in the former case, obtaining that

$$\int_D |\nabla^2 w_0|^2 \geq \frac{12}{26^2} a^2 |D|. \tag{82}$$

Therefore, from Proposition 3.2, (75) and (82), we have the following upper bounds for the relative measure of stiff inclusions

$$\frac{|D|}{|\Omega|} \leq \left(\frac{169f}{(f-1)(1-\nu)} \right) \frac{W_0 - W}{W_0}, \tag{83}$$

and soft inclusions

$$\frac{|D|}{|\Omega|} \leq \left(\frac{169}{(1-f)(1-\nu)} \right) \frac{W - W_0}{W_0}, \tag{84}$$

respectively.

4.2. **Finite element model for Kirchhoff–Love plate.** In order to numerically assess the capabilities of the energy gap in the estimation of the inclusion size, a series of finite element analysis have been performed. The choice of the *optimal* finite element derives from the balance between the computation cost related to the large of numerical simulations to be performed and the accuracy in the evaluation of the work gap. This choice arises from the following considerations:

(1) triangular elements have to be preferred since they are capable to better describe general shape inclusions;
(2) appropriate plate elements have to be able to impose C^1 inter-element continuity, at least in relaxed form;
(3) moderately fine meshes have to be anyway used in order to represent as accurate as possible the considered inclusion.

Consequently, all the problems considered in the numerical experimentation have been discretized on the basis of a three-node triangular element defined in the Specht's paper, see [27] for an in-depth discussion, useful for general application to elastic Kirchhoff–Love plates.

Specht's element is a refinement of a triangular finite element which uses polynomial displacement basis for the three-node plate bending element, proposed initially by Zienkiewicz [33] and improved successively

by Bergan [34], obtained by relaxing the C^1 inter-element continuity. In this way the Specht's element overcomes the *patch test* without paying the price of more sophisticated, therefore more expensive in computational terms, elements.

This finite element is defined by the out-of-plane displacements and by the two rotation of the nodes collocated in the triangle vertices in such a way that these nine parameters describe univocally the transversal displacement of the plate by means of a polynomial expansion complete up to the second order plus three terms taking into account the third- and fourth-order contributions. More precisely, the Ritz interpolating space is defined as follows:

$$\begin{aligned}\mathbf{P} = \{&\xi_1, \xi_2, \xi_3, \xi_1\xi_2, \xi_2\xi_3, \xi_3\xi_1,\\ &\xi_1^2\xi_2 + \frac{1}{2}\xi_1\xi_2\xi_3(3(1-\mu_3)\xi_1 - (1+3\mu_3)\xi_2 + (1+3\mu_3)\xi_3),\\ &\xi_2^2\xi_3 + \frac{1}{2}\xi_1\xi_2\xi_3(3(1-\mu_1)\xi_2 - (1+3\mu_1)\xi_3 + (1+3\mu_1)\xi_1),\\ &\xi_3^2\xi_1 + \frac{1}{2}\xi_1\xi_2\xi_3(3(1-\mu_2)\xi_3 - (1+3\mu_2)\xi_1 + (1+3\mu_2)\xi_2)\}\,,\end{aligned} \tag{85}$$

where ξ_i, ξ_j, ξ_k are the area coordinates of the element ($\xi_i+\xi_j+\xi_k = 1$), see Fig. 1, the parameters

$$\mu_1 = \frac{\ell_3^2 - \ell_2^2}{\ell_1^2}, \qquad \mu_2 = \frac{\ell_1^2 - \ell_3^2}{\ell_2^2}, \qquad \mu_3 = \frac{\ell_2^2 - \ell_1^2}{\ell_3^2} \tag{86}$$

depend from the lengths ℓ_i, ℓ_j,ℓ_k of the triangle edges and A is the area of the element, see again Figure 1.

The finite element just defined, beyond to overcome the patch test, is characterized by a good computational performance as is reported in [27]. Generally speaking, few elements allow to reach a reasonable accuracy. However, it necessary to point out that in our simulations the mesh grain is surely more refined than the necessary in order to have the resolution necessary to highlight the considered inclusion size.

The finite element implementation used in the numerical simulations

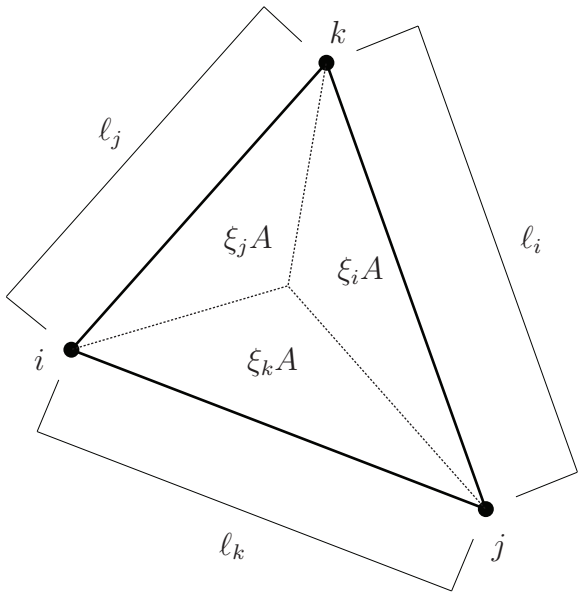

FIGURE 1. Specht's triangular finite element: nodes (i, j,k), edge lengths (ℓ_i, ℓ_j,ℓ_k) and area partitions ($\xi_i A$, $\xi_j A$,$\xi_k A$).

has been tested on the basis of some standard thin plate problems. The analyses concern a square plate uniformly loaded and subjected to the following boundary conditions:

Problem 1**:** simply-supported on all edges;

Problem 2**:** simply-supported on two opposite edges and built-in for the other ones;

Problem 3**:** built-in on all edges.

For the considered problems a indicates the edge length of the plate, h its thickness, q the applied uniform load and $B = \frac{Eh^3}{12(1-\nu^2)}$ the bending stiffness of the plate in terms of the Young's modulus E and the Poisson's ratio ν. The used meshes are based on the subdivision of each field, with t size of a regular grid, in two parts, see Figure 2. In

this way the mesh is uniquely determined by the grain mesh parameter $\eta = a/t$ which give immediately the number of elements, equal to $2\eta^2$, and the numbers of nodes n_N, equal to $(\eta + 1)^2$. Figure 3 reports the

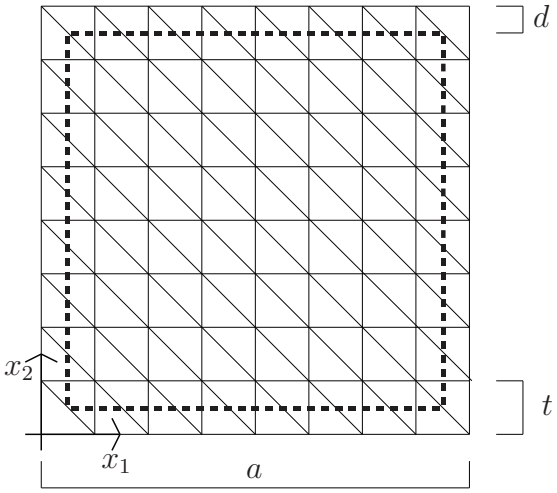

FIGURE 2. Finite element discretization of level $\eta = a/t$ for a square domain ($\eta = 8$ in this case).

error, in percentage, for normalized values of the maximum displacement $w_{\max}B/qa^4 - 1$ of the plates and Figure 4 shows the convergence of the strain energy of the plate W_0 to the exact value W_0^* as reported in [35]. Results reported in Figures 3 and 4 furnished the guidelines to choice of the mesh size for the following simulations.

4.3. **Description of the results.**

4.3.1. *Case i): bending moments along all the edges.* Figure 5 reports, besides the sketch of the problem and its boundary conditions (Fig. 5(a)), the normalized work gap $(W - W_0)/W_0$ with respect to the position of a single 1×1 square inclusion. The graph has been obtained by interpolating the discrete values of the gap, assigned on the centroids of the inclusions, and highlights that the position of the inclusion slightly

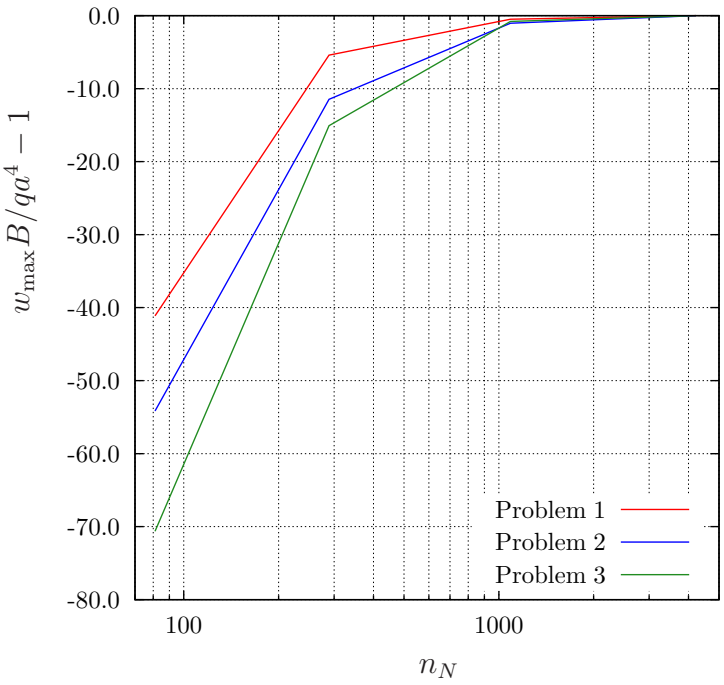

FIGURE 3. Computed error on normalized maximum displacements $w_{\max} b/qa^4 - 1$, in percentage, with respect to the number of the nodes n_N of the mesh.

affects the energy gap. The fact that the work gap is rather insensitive with respect to the position of such small inclusions is consistent with the predictions of the topological derivative approach, see, among other contributions, [36] and [37]. Similar considerations apply to next cases ii) and iii), see Figures 10 and 14, respectively. Figure 6 shows the results obtained for three choices of the parameter d, which represents the minimal distance between inclusions and boundary. In particular, the choices $d/a = 0.038$ and $d/a = 0.115$ correspond to the removal of one and three rows of square elements near the boundary, respectively.

Figure 7 shows the effect of different values of the stiffness ratio f relative to square stiff inclusions, Fig. 7(a), and square soft inclusions,

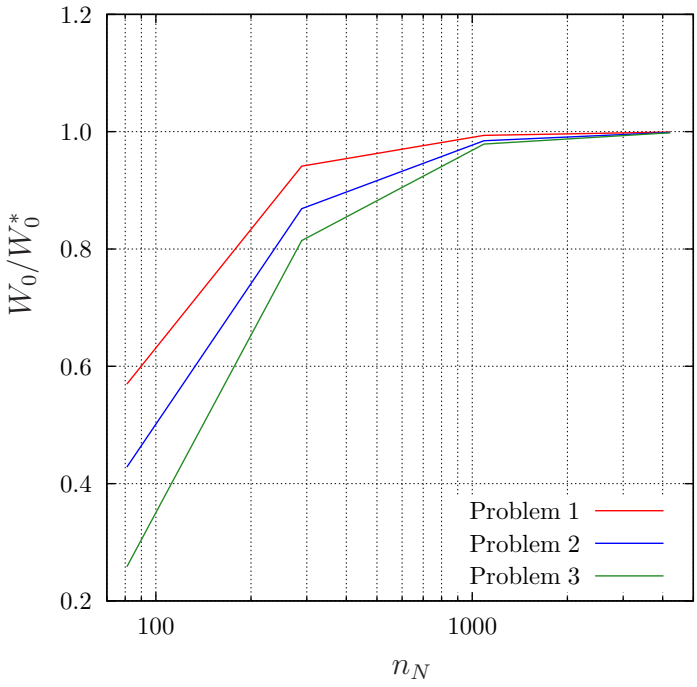

FIGURE 4. Computed normalized strain energies W_0/W_0^* with respect to the number of nodes n_N of the mesh.

Fig. 7(b). Results have been obtained by using a mesh based on a 26×26 grid and $d/a = 0.115$. According to the theory, and noticing that hypothesis (62) is obviously satisfied, the points $(|W - W_0|/W_0, |D|/|\Omega|)$ belong to the angular sector defined by the two straight lines representing the analytical bounds (71) and (72), for stiff and soft inclusions, respectively.

The study of inclusions of more general shape involves a very large number of simulations and therefore it would require an excessive computational burden. Therefore, to make the numerical analysis sustainable in practice, we have implemented an automatic generator of subdomains. Specifically, the inclusions have been generated starting from a triangular element placed at the center of the plate and adding

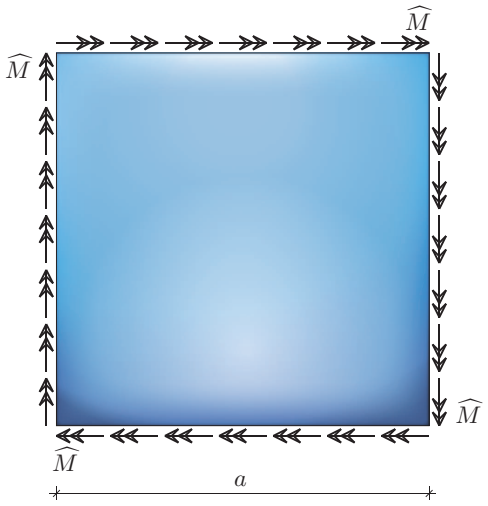

(a)

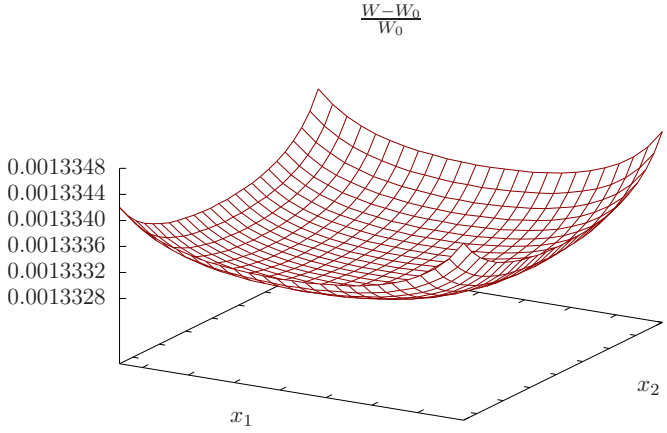

(b)

FIGURE 5. Case i). Plate subject to constant distribution of bending moments on the boundary (a); normalized work gap $(W - W_0)/W_0$ in terms of the position of a single 1×1 square inclusion, with $f = 0.2$, $|D|/|\Omega| = 6.25 \cdot 10^{-4}$ and mesh based on a 40×40 grid (b).

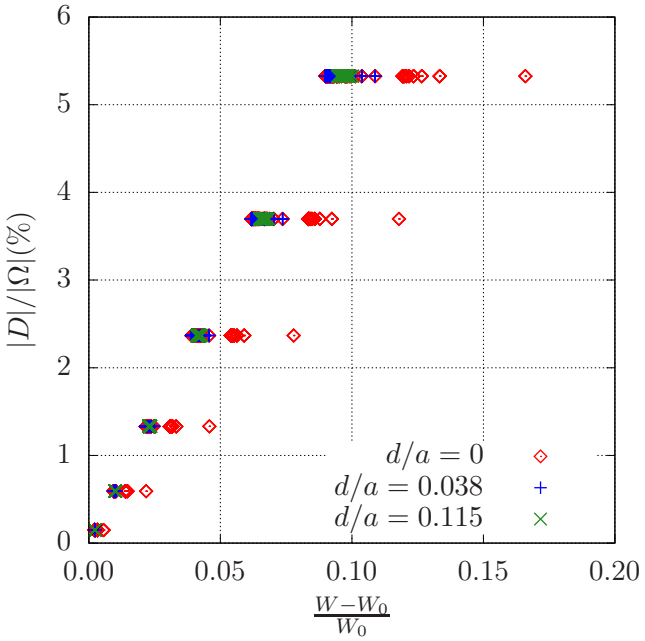

FIGURE 6. Case i). Plate subject to a constant distribution of bending moments on the boundary: influence of the geometrical parameter d for soft square inclusions ($f = 0.2$) on a mesh based on a 26×26 grid.

adjacent elements to obtain families with a given area $|D|$, see, for example, Figure 8 for inclusions made by one, two and three triangular elements. The analysis has been restricted to a mesh based on a 18×18 grid and the automatic generation has been extended up to the family with 16 triangular elements. In spite of this coarse mesh, the number of inclusions to be considered is significantly high. Indeed, the plot of Figure 9(a), in which a comparison with the case of square inclusion is proposed, required 63365 simulations. In Figure 9(b) the data are collected on the basis of the normalized iso-perimetric deficit of the inclusion defined as

$$I_d = \frac{P^2 - 4\pi A}{4\pi A}\,, \tag{87}$$

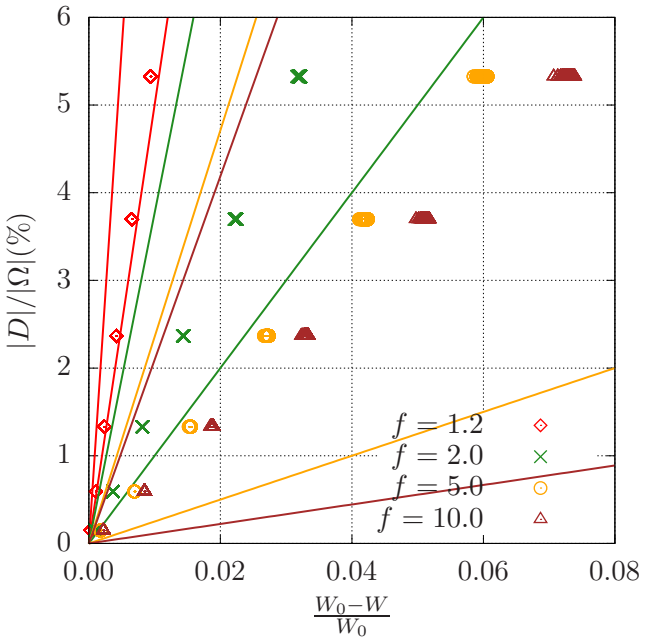

(a)

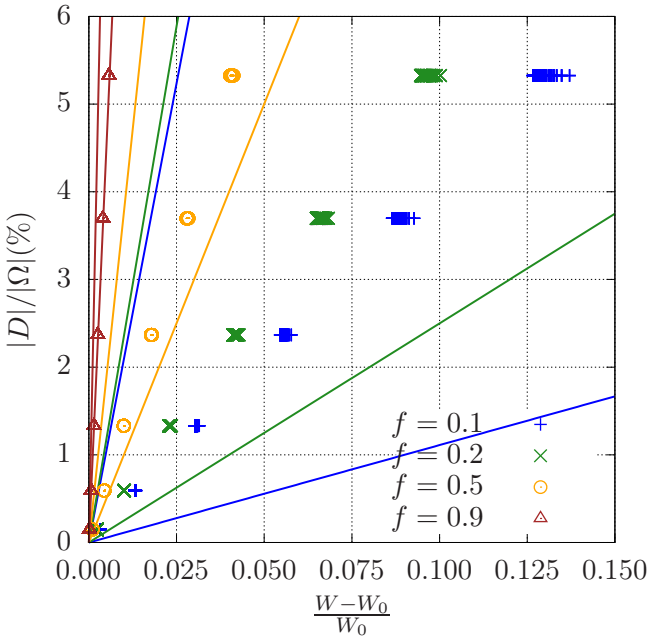

(b)

FIGURE 7. Case i). Plate subject to constant distribution of bending moments on the boundary: influence of the stiffness ratio f for square inclusions with $d/a = 0.115$ and mesh based on a 26×26 grid; stiff (a) and soft (b) inclusions.

where P and A are, respectively, the perimeter and the area of the inclusion. It should be recalled that $I_p = 0$ and $I_p = 0.273$ for a disc and a square, respectively.

In Figure 9 we have also drawn the two straight lines whose slope represents the numerical value of the constants appearing in the theoretical size estimates. It clearly emerges that the theoretical bounds are rather pessimistic, see also Table 1.

TABLE 1. Comparison for the case study i)-iv) between the slopes defining the lines for the theoretical lower and upper bounds, L_t and U_t respectively, and the numerical ones, L_n and U_n for soft inclusions ($f = 0.2$).

case	L_t	U_t	L_n	U_n
i)	0.2500	2.3552	0.3995	0.6400
ii)	0.1606	1.5125	0.3853	1.1300
iii)	0.1346	1.2682	0.6236	1.0353
iv)	0.0641	301.48	0.4450	55.000

4.3.2. *Case ii): bending moments along two opposite edges.* In this case, bending moments of constant amplitude are applied along two opposite edges of the plate, see Figure 10(a). Figure 10(b) shows the variation of the normalized energy gap $(W - W_0)/W_0$ with respect to the position of a square inclusion of fixed size.

The effect of the geometrical parameter d has been highlighted in Figure 11 for stiffness ratio $f = 0.2$, whereas Figure 12 shows the influence of different choices of f. The latter two analyses have been performed for square inclusions in a mesh based on a 26×26 grid. Finally, Figure 13(a) reports the results for inclusions of general shape,

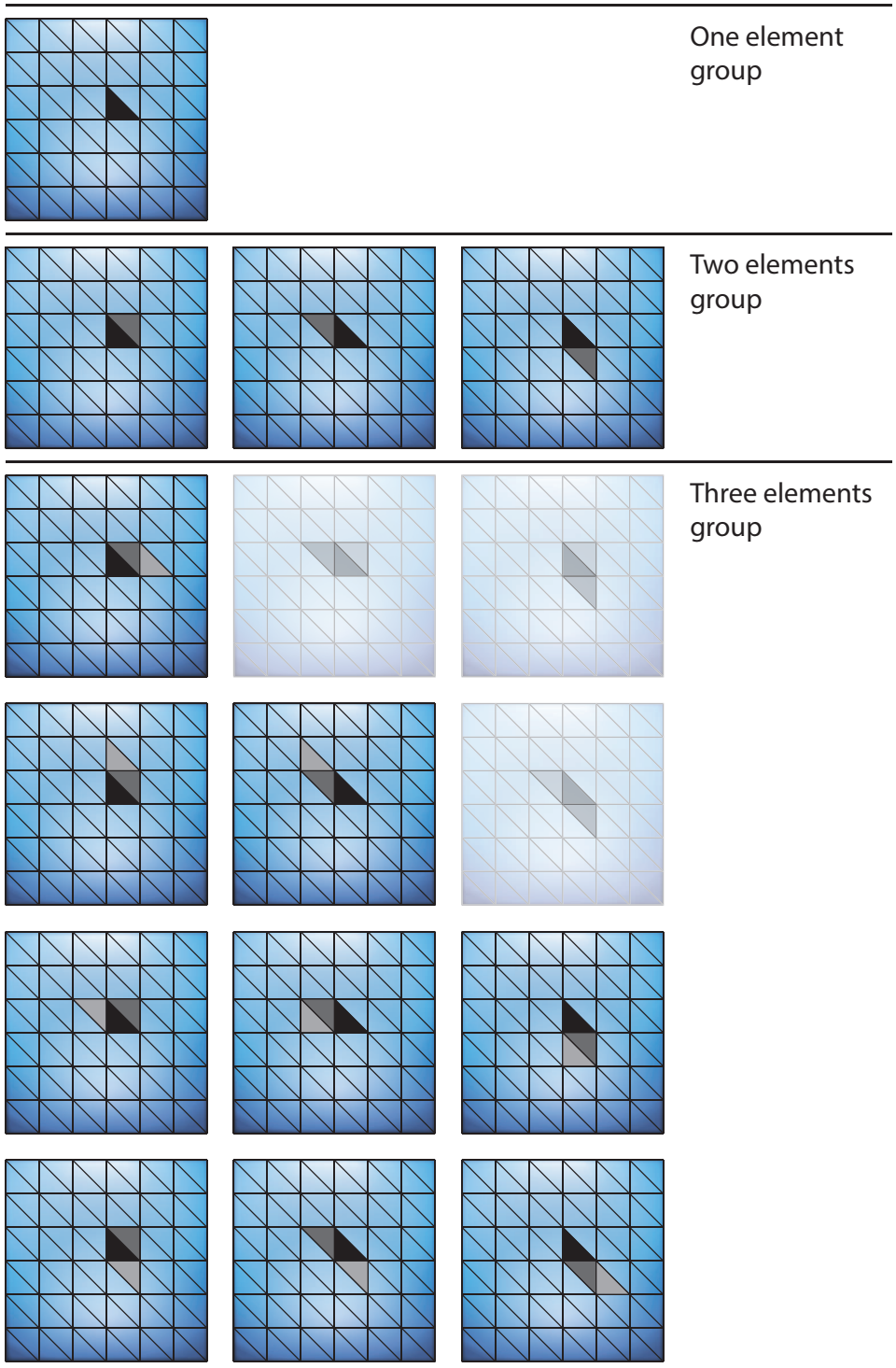

FIGURE 8. First three families of inclusions generated from the center of the plate (repeated patterns are shown using light color).

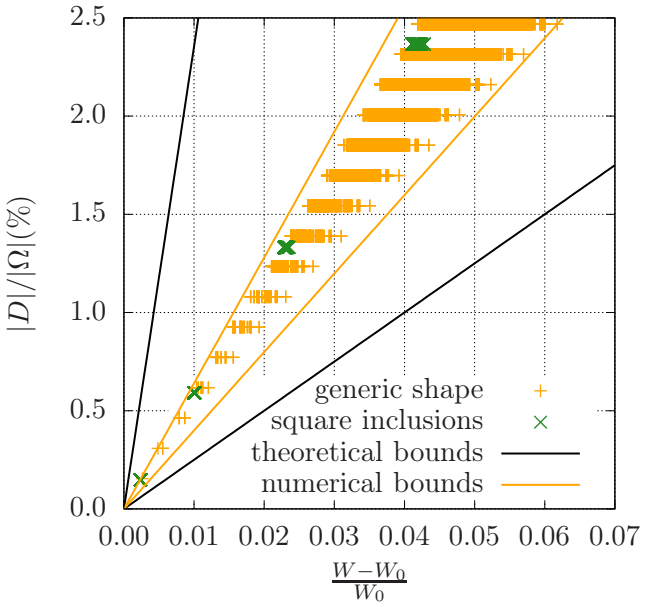

(a)

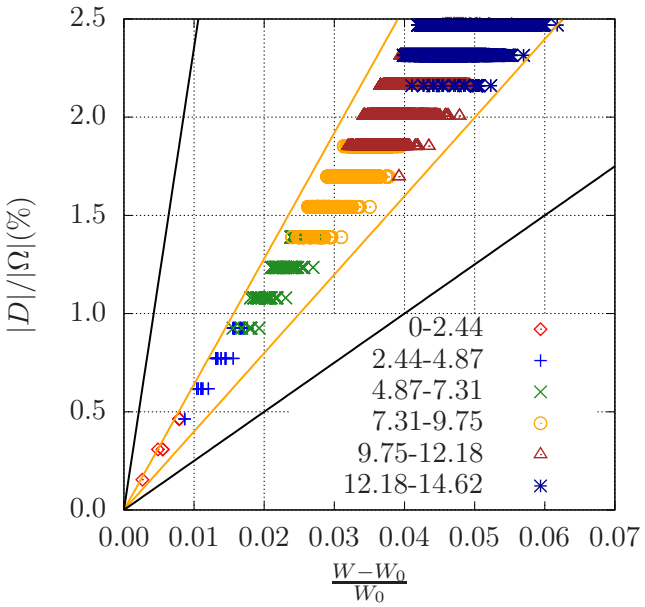

(b)

FIGURE 9. Case i). Plate subject to constant distribution of bending moments on the boundary: comparison between square inclusions (mesh based on a 26×26 grid, $d/a = 0.115$) and inclusions of generic shape (mesh based on a 18×18 grid, $d/a = 0.115$) with $f = 0.2$ (a); influence

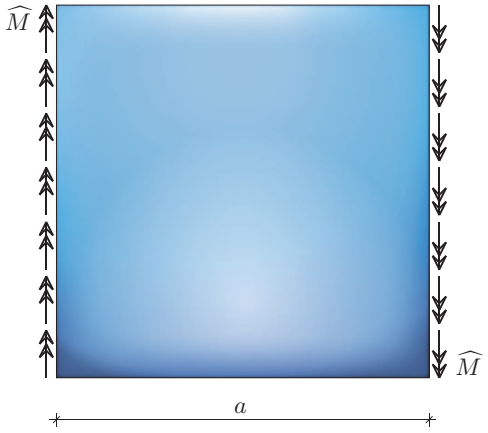

(a)

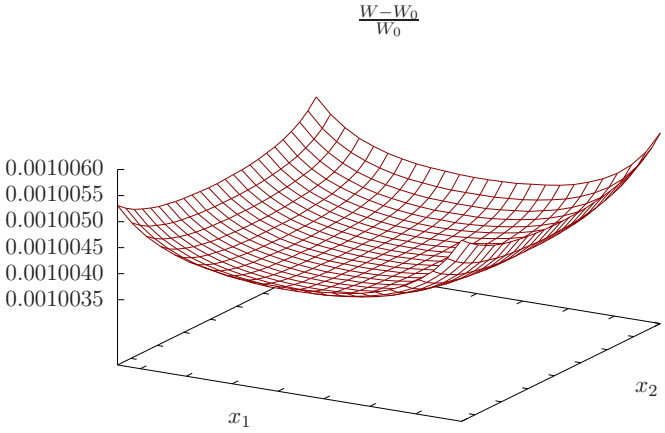

(b)

FIGURE 10. Case ii). Plate subject to constant distribution of bending moments along two opposite edges (a); normalized work gap $(W - W_0)/W_0$ in terms of the position of a single 1×1 square inclusion, with $f = 0.2$, $|D|/|\Omega| = 6.25 \cdot 10^{-4}$ and mesh based on a 40×40 grid (b).

and Figure 13(b) highlights the role of the normalized iso-perimetric deficit I_d.

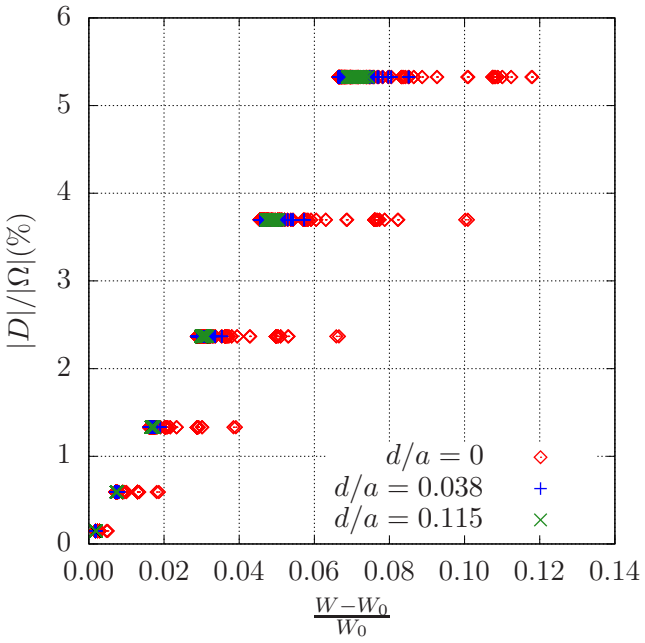

FIGURE 11. Case ii). Plate subject to constant distribution of bending moments along two opposite edges: influence of the parameter d for square inclusions, with $f = 0.2$ and mesh based on a 26×26 grid.

Overall, the results are qualitatively similar to the previous ones, the only significant difference being that the sector obtained for soft inclusions of generic shape (with $f = 0.2$) is wider than the corresponding sector obtained in case i); compare Figures 9(a) and 13(a).

4.3.3. *Case iii): twisting moments along two opposite edges.* The normalized work gap $(W - W_0)/W_0$ with respect to the position of a square inclusion of fixed size is reported in Figure 14(b) for $f = 0.2$ and a mesh based on a 40×40 grid.

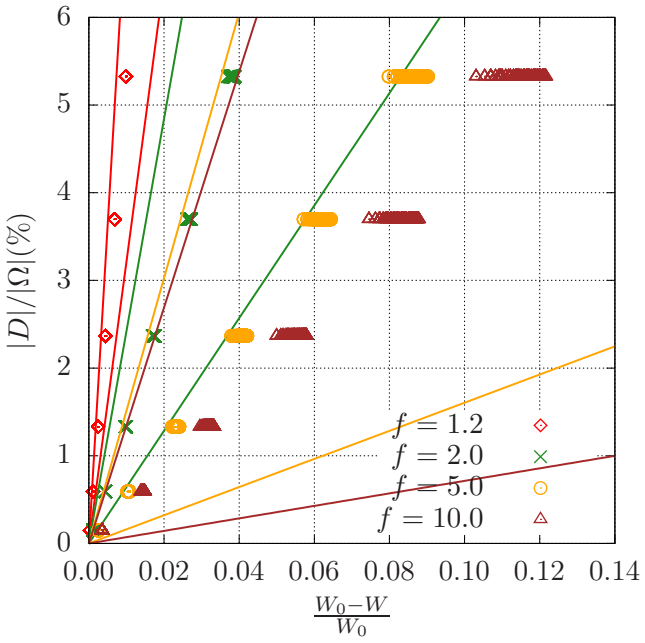

(a)

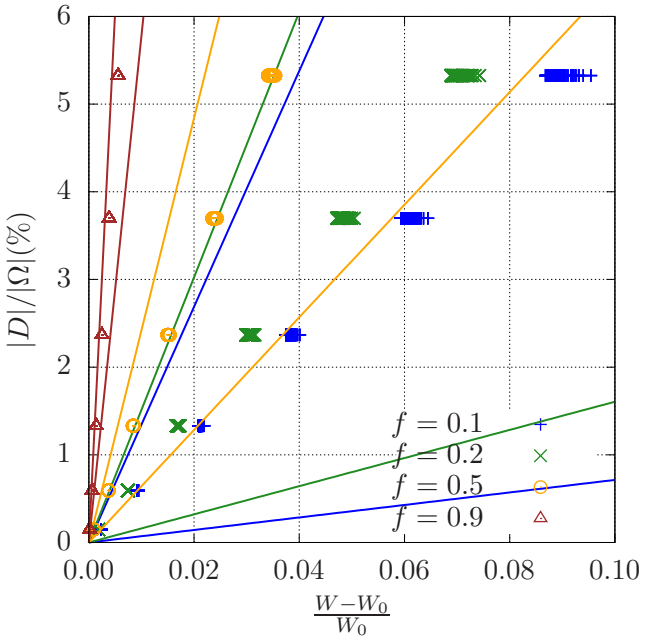

(b)

FIGURE 12. Case ii). Plate subject to constant distribution of bending moments along two opposite edges: influence of the stiffness ratio f for square inclusions, with $d/a = 0.115$ and mesh based on a 26×26 grid; stiff (a) and soft (b) inclusions.

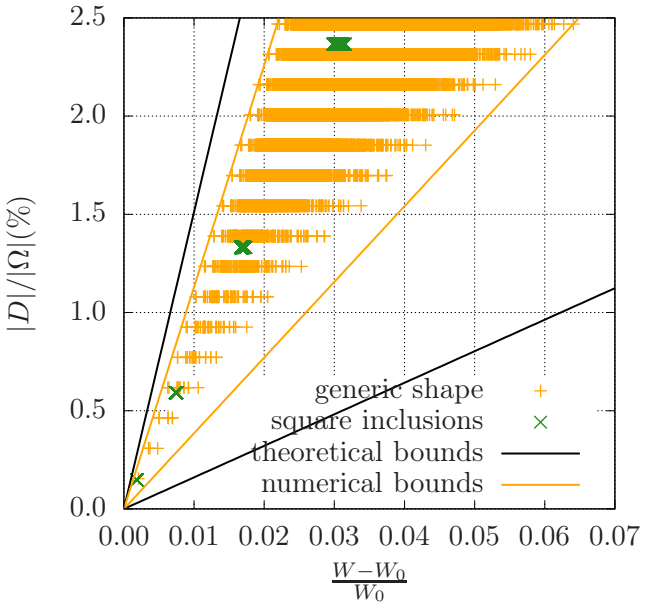

(a)

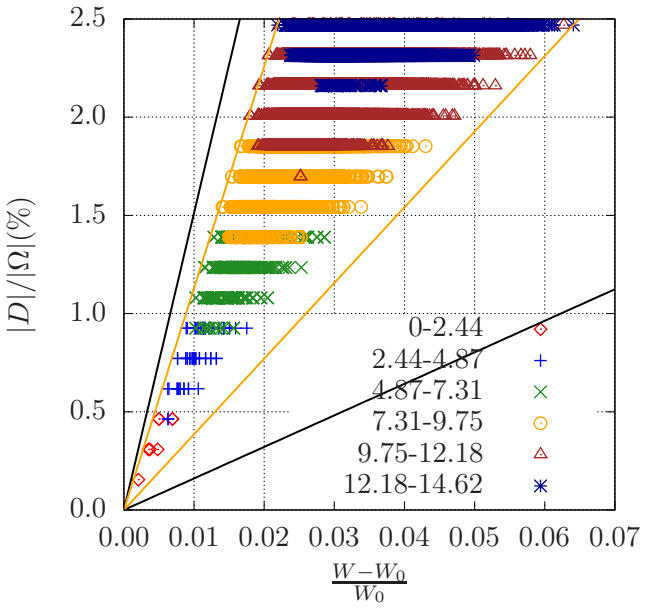

(b)

FIGURE 13. Case ii). Plate subject to constant distribution of bending moments along two opposite edges: comparison between square inclusions (26×26 mesh, $d/a = 0.115$) and inclusions of generic shape (18×18 mesh, $d/a = 0.115$), with $f = 0.2$ (a); influence of the

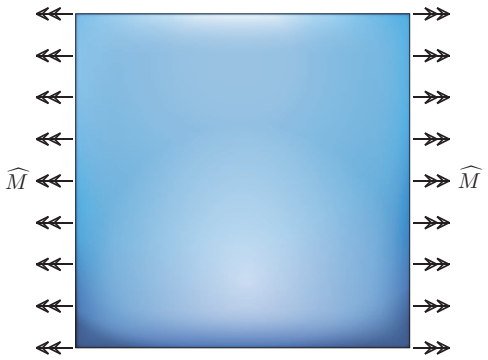

(a)

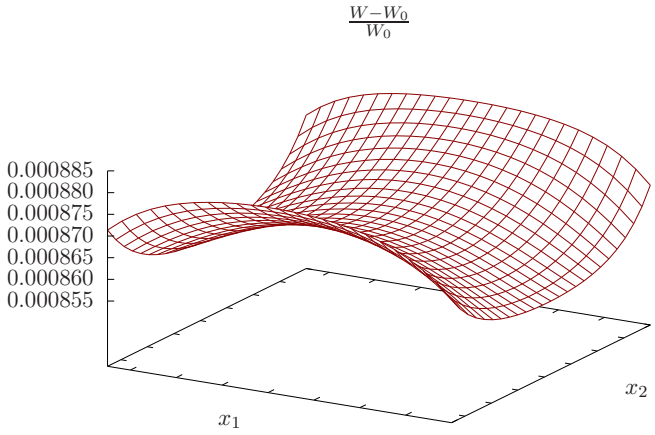

(b)

FIGURE 14. Case iii). Plate subject to constant distribution of twisting moments along two opposite edges (a); normalized work gap $(W - W_0)/W_0$ in terms of the position of a single 1×1 square inclusion, with $f = 0.2$, $|D|/|\Omega| = 6.25 \cdot 10^{-4}$ and mesh based on a 40×40 grid (b).

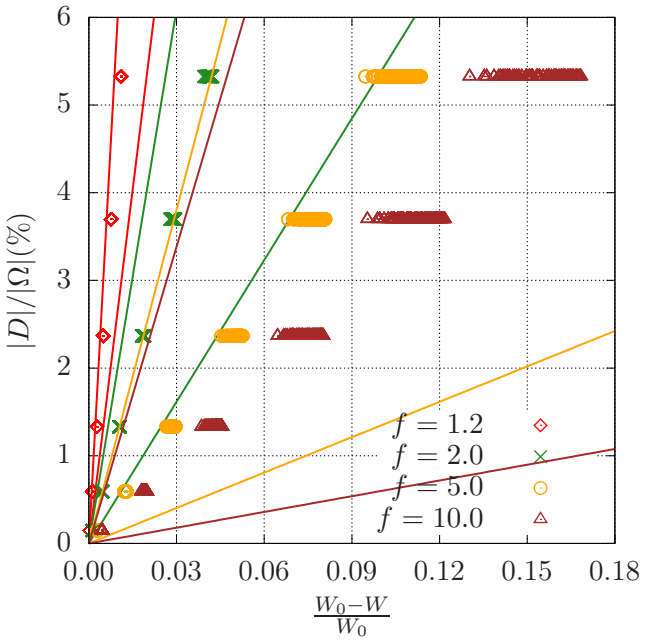

(a)

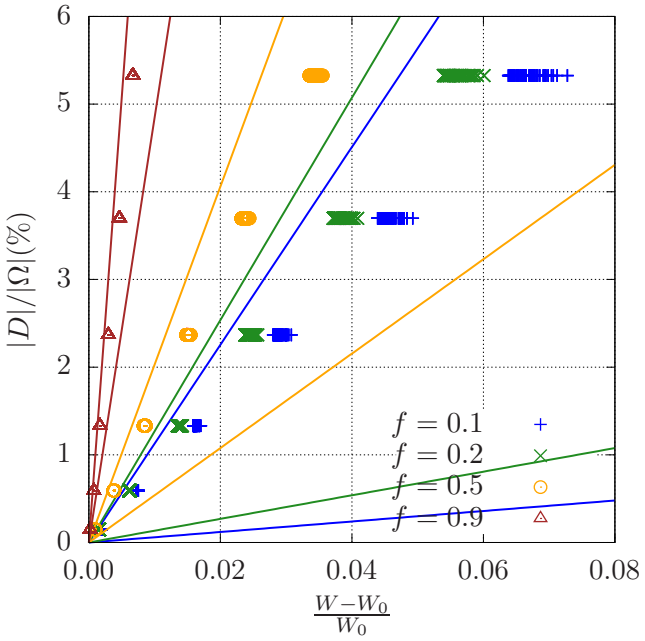

(b)

FIGURE 15. Case iii). Plate subject to constant distribution of twisting moments along two opposite edges: influence of the stiffness ratio f for square inclusions, with $d/a = 0.115$ and mesh based on a 26×26 grid; stiff (a) and soft (b) inclusions.

The effect of the stiffness ratio f is investigated in Figure 15. Figure 16 summarizes the result obtained for inclusions of general shape.

Compared to the previous cases i) and ii), the results of the numerical simulations seem to show a lower sensitivity of the work gap for soft inclusions. The opposite happens for rigid inclusions.

4.3.4. *Case iv): Hessian vanishing along* $x_1 = a/2$. As for the foregoing cases, Figure 17 reports the boundary conditions (Fig. 17(a)) and the normalized work gap $(W - W_0)/W_0$ evaluated for a single 1×1 square inclusion (Fig. 17(b)), with $f = 0.2$ and a mesh based on a 40×40 grid. Figure 17(b) shows that the normalized work gap is minimal and close to zero when the 1×1 square inclusion is adjacent to the line $x_1 = a/2$. The effect of the stiffness ratio f is investigated in Figure 18.

Figure 19 compares the result obtained for square and general shape inclusions. The influence of the iso-perimetric deficit I_d is analysed in Fig. 19(b). Figure 20, in particular, is a blow-up of Fig. 19(a) near the origin, which is useful for estimating the upper bound of the size estimates.

Figure 21 shows the results obtained by considering generic shapes formed by groups of n elements with $n = 1, \dots, 9$. Only for the groups with $n = 4, \dots, 9$, shapes which give the maximum and minimum values of the energy gap are highlighted. This figure points out that the presence of an inclusion near the zeroes of $\nabla^2 w_0$ gives rise to small normalized work gap, which could obstruct its identification. It is worth noting how the condition of a zero contribution to the elastic energy for the points of the plate belonging to the line $x = a/2$ forces the elements of the groups with the minimum energy gap to take a position on both sides of this line.

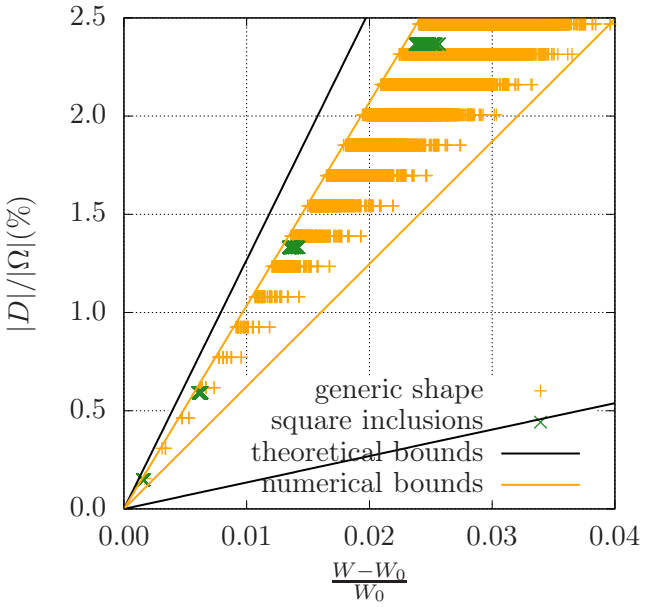

(a)

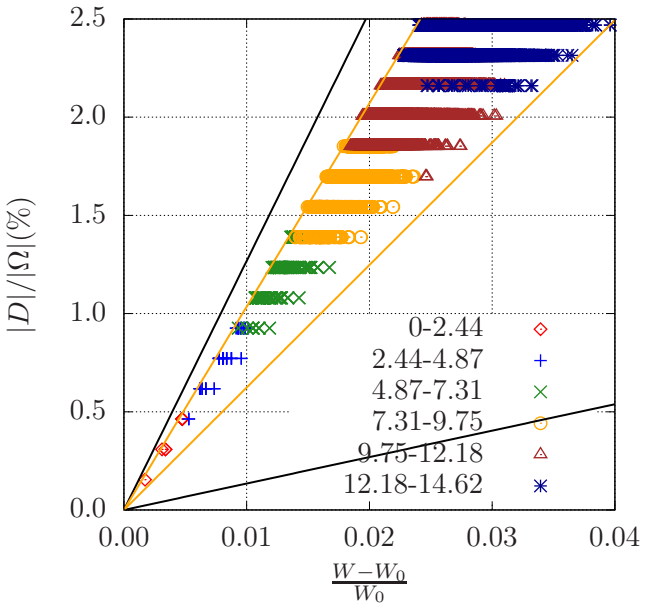

(b)

FIGURE 16. Case iii). Plate subject to constant distribution of twisting moments along two opposite edges: comparison between square inclusions (26×26 grid, $d/a = 0.115$) and inclusions of generic shape (18×18 grid, $d/a = 0.115$) with $f = 0.2$ (a); influence of the

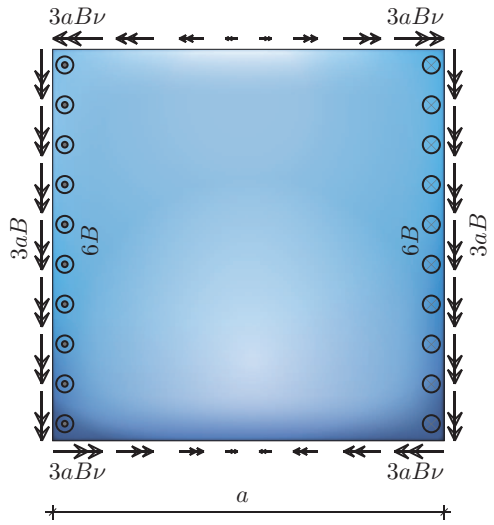

(a)

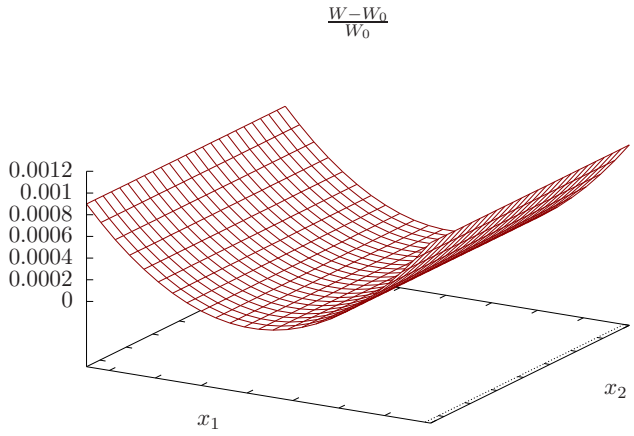

(b)

FIGURE 17. Case iv). Plate with Hessian vanishing along $x_1 = a/2$: geometry and boundary conditions (a) and normalized work gap $(W - W_0)/W_0$ in terms of the position of a single 1×1 square inclusion with $f = 0.2$, $|D|/|\Omega| = 6.25 \cdot 10^{-4}$ and mesh based on a 40×40 grid (b).

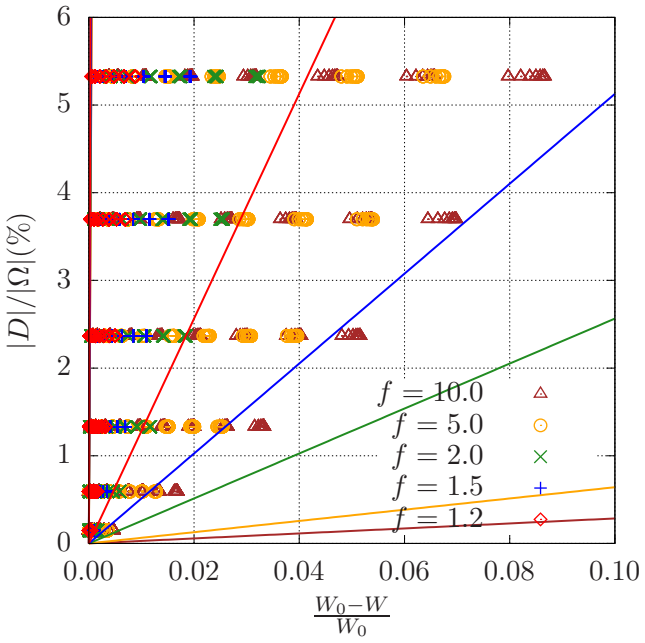

(a)

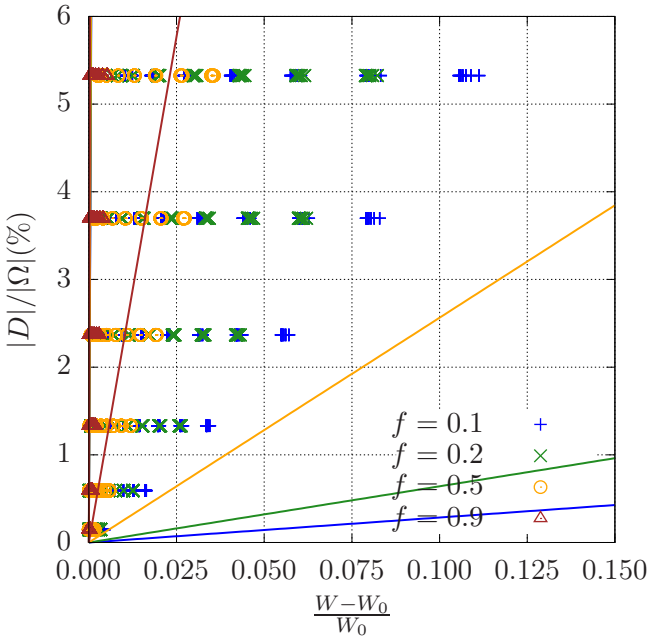

(b)

FIGURE 18. Case iv). Hessian vanishing along $x_1 = a/2$: influence of the stiffness ratio f for square inclusions with $d/a = 0.115$ and mesh based on a 26×26 grid; stiff (a) and soft (b) inclusions.

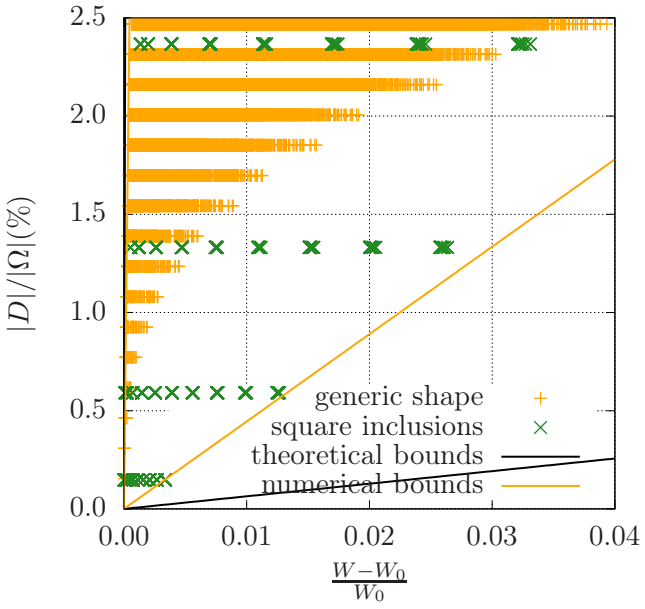

(a)

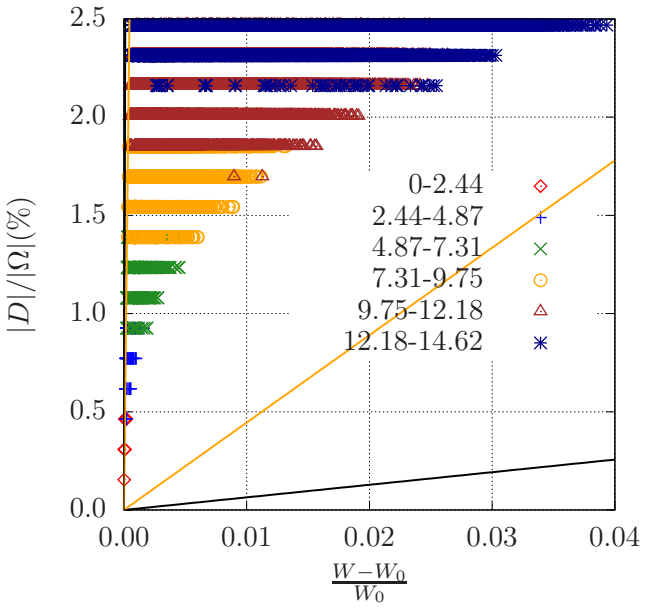

(b)

FIGURE 19. Case iv). Hessian vanishing along $x_1 = a/2$: comparison between square inclusions (26×26 mesh) and inclusions of generic shape (18×18 mesh), with $f = 0.2$ (a); influence of the normalized iso-perimetric deficit I_d (b).

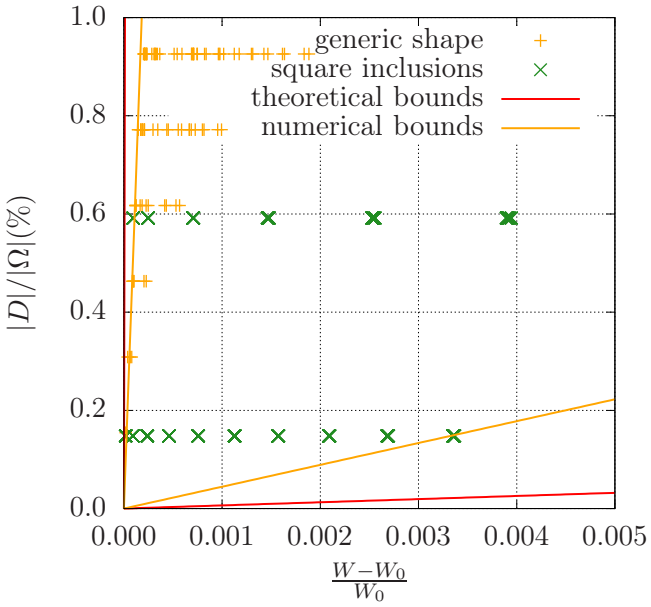

FIGURE 20. Case iv). Hessian vanishing along $x_1 = a/2$: blow-up of the comparison between square inclusions (26×26 mesh) and inclusions of generic shape (18×18 mesh), with $f = 0.2$.

5. Concluding remarks

In this paper we tested by numerical simulations the size estimates approach for the identification of inclusions in Kirchhoff-Love elastic plates. In previous works [17] and [18] it was shown how upper and lower bounds of the area of an unknown elastic inclusion inside a thin elastic plate can be obtained in terms of the difference between the work exerted by a boundary couple field when the inclusion is present or absent. The analytical procedure behind these theoretical estimates typically leads to rather pessimistic evaluations of the constants appearing in the size estimates. Therefore, with a view to practical applications of

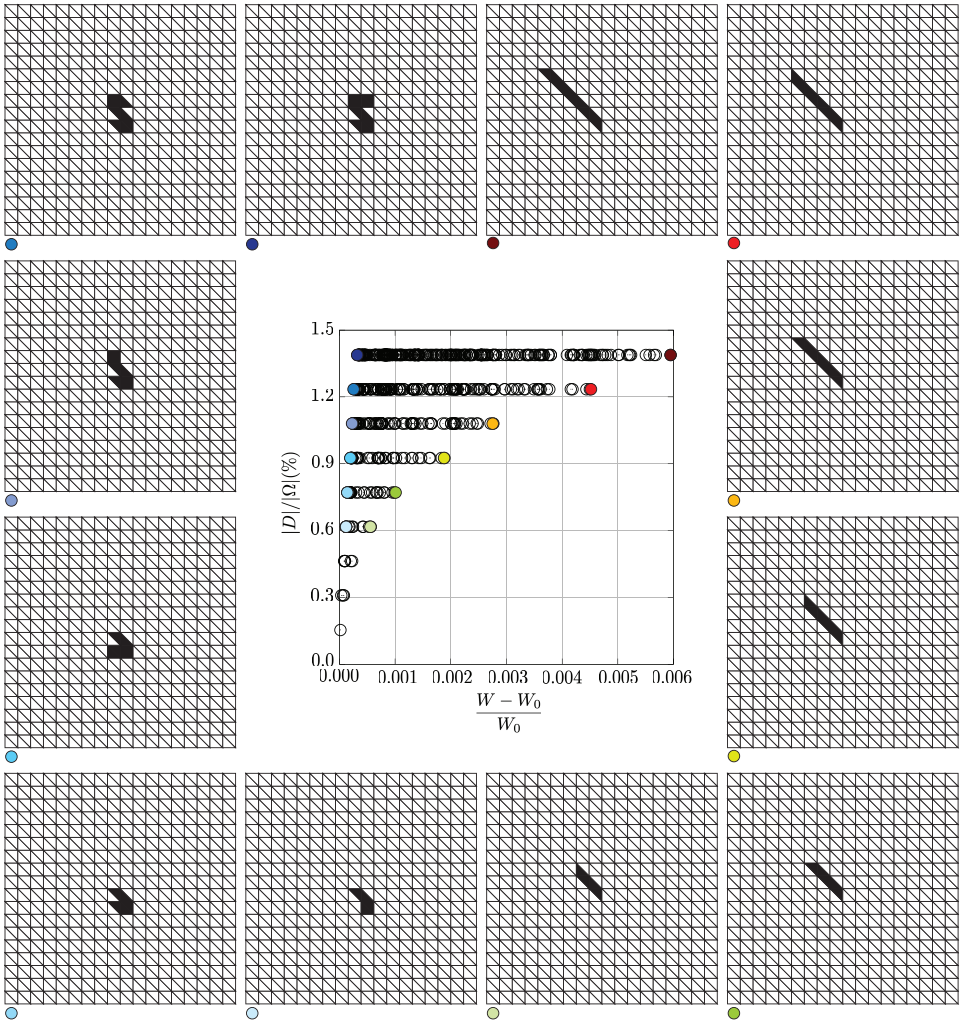

FIGURE 21. Case iv). Hessian vanishing along $x_1 = a/2$: pattern of inclusions which produce extremal values of the work gap.

the size estimates approach as diagnostic tool, in this paper we focused on the quantitative evaluation of such constants in some test cases.

An extended series of numerical simulations has been carried out on a square plate subject to different sets of boundary conditions. The results of the tests performed confirm that the theoretical predictions of the bounds are rather pessimistic. Moreover, the numerical analysis

allowed to quantify how the constants appearing in the lower and upper size estimates are influenced by some significant parameters of the problem, such as the position, the shape and the stiffness of the inclusion. Another important aspect emerging from computations concerns the role played by the load distribution applied on the boundary of the specimen. It has been verified that when the boundary couple field produces regions of vanishing strain energy inside the plate, the upper bound deteriorates. This may give a useful indication on the choice of the loading distribution for practical applications of the method.

Acknowledgements

(1) The Authors wish to thank the unknown Referee for her/his constructive work and helpful comments.
(2) E. Rosset acknowledges the financial support of GNAMPA 2017 and 2018 of the Istituto Nazionale di Alta Matematica (INdAM) and of FRA2016 “Problemi inversi, dalla stabilità alla ricostruzione”, Università degli Studi di Trieste.
(3) A. Morassi acknowledges the financial support of the National Research Project PRIN 2015TT JN95 “Identification and monitoring of complex structural systems”.
(4) S. Vessella acknowledges the financial support of GNAMPA 2017 and 2018 of the Istituto Nazionale di Alta Matematica (INdAM).

References

[1] M. Bonnet and A. Constantinescu. Inverse problems in elasticity. *Inverse Problems*, 21(2):1–50, 2005.

[2] A. Morassi and F. Vestroni, editors. *Dynamic methods for damage detection in structures*, volume 499 of *CISM International Centre for Mechanical Sciences*. Springer, Wien, 1st edition, 2008.

[3] U. Lee, K. Cho, and J. Shin. Identification of orthotropic damages within a thin uniform plate. *International Journal of Solids and Structures*, 40(9):2195–2213, 2003.

[4] S. Caddemi, I. Caliò, F. Cannizzaro, and A. Morassi. A procedure for the identification of multiple cracks on beams and frames by static measurements. *Structural Control & Health Monitoring*, 25(8):e2194, 2018.

[5] P.-L. Liu and H.-T. Lin. Direct identification of non-uniform beams using static strains. *International Journal of Solids and Structures*, 33(19):2775–2787, 1996.

[6] P. Cornwell, S. W. Doebling, and C. R. Farrar. Application of the strain energy damage detection method to plate-like structures. *Journal of Sound and Vibration*, 224:359–374, 1999.

[7] Y. Y. Li, L. Cheng, L. H. Yam, and W. O. Wong. Identification of damage locations for plate-like structures using damage sensitive indices: strain modal approach. *Computers and Structures*, 80:1881–1894, 2002.

[8] G. Fichera. *Existence Theorems in Elasticity*, volume VI of *Handbuch der Physik*, pages 347–389. Springer-Verlag, Berlin, Heidelberg, 1972.

[9] P. G. Ciarlet. *Mathematical Elasticity: Theory of Shells*, volume II. North-Holland Publishing Co., Amsterdam, 2000.

[10] G. Alessandrini. Generic uniqueness and size estimates in the inverse conductivity problem with one measurement. *Matematiche (Catania)*, 54:5–14, 1999.

[11] V. Isakov. *Inverse Problems for Partial Differential Equations*. Springer, New York, 1998.

[12] G. Alessandrini and E. Rosset. The inverse conductivity problem with one measurement: bounds on the size of the unknown object. *SIAM Journal on Applied Mathematics*, 58:1060–1071, 1998.

[13] H. Kang, J. K. Seo, and D. Sheen. The inverse conductivity problem with one measurement: stability and estimation of size. *SIAM Journal on Mathematical Analysis*, 28:1389–1405, 1997.

[14] G. Alessandrini, E. Rosset, and J. K. Seo. Optimal size estimates for the inverse conductivity problem with one measurement. *Proceedings of American Mathematical Society*, 128:53–64, 2000.

[15] M. Ikehata. Size estimation of inclusion. *Journal of Inverse and Ill-Posed Problems*, 6:127–140, 1998.

[16] G. Alessandrini, A. Morassi, and E. Rosset. Detecting an inclusion in an elastic body by boundary measurements. *SIAM Journal on Mathematical Analysis*, 33(6):1247–1268, 2002.

[17] A. Morassi, E. Rosset, and S. Vessella. Size estimates for inclusions in an elastic plate by boundary measurements. *Indiana University Mathematics Journal*, 56(5):2325–2384, 2007.

[18] M. Di Cristo, C.-L. Lin, A. Morassi, S. Vessella, and J.-N. Wang. Doubling inequalities for anisotropic plate equations and applications to size estimates of inclusions. *Inverse Problems*, 29:125012, 2013.

[19] A. Morassi, E. Rosset, and S. Vessella. Recent results about the detection of unknown boundaries and inclusions in elastic plates. *Journal of Inverse and Ill-Posed Problems*, 21(2):311–352, 2013.

[20] M. Di Cristo, C. L. Lin, and J. N. Wang. Quantitative uniqueness estimates for the shallow shell system and their application to an inverse problem. *Annali della Scuola Normale Superiore di Pisa, Classe di Scienze*, 12:43–92, 2013.

[21] M. Di Cristo, C. L. Lin, S. Vessella, and J. N. Wang. Size estimates of the inverse inclusion problem for the shallow shell equation. *SIAM Journal on Mathematical Analysis*, 45:88–100, 2013.

[22] A. Morassi, E. Rosset, and S. Vessella. Size estimates for fat inclusions in an isotropic Reissner–Mindlin plate. *Inverse Problems*, 34:025001, 2018.

[23] Y. Capdeboscq and M. S. Vogelius. Optimal asymptotic estimates for the volume of internal inhomogeneities in terms of multiple boundary measurements. *Mathematical Modelling and Numerical Analysis*, 37:227–240, 2003.

[24] G. Alessandrini, A. Bilotta, A. Morassi, E. Rosset, and E. Turco. Computing volume bounds of inclusions by EIT measurements. *Journal of Scientific Computing*, 33(3):293–312, 2007.

[25] G. Alessandrini, A. Bilotta, G. Formica, A. Morassi, E. Rosset, and E. Turco. Numerical size estimates of inclusions in elastic bodies. *Inverse Problems*, 21:133–151, 2005.

[26] G. Alessandrini, A. Bilotta, G. Formica, A. Morassi, E. Rosset, and E. Turco. Evaluating the volume of a hidden inclusion in an elastic body. *Journal of Computational and Applied Mathematics*, 198(2):288–306, 2007.

[27] B. Specht. Modified shape functions for the three-node plate bending element passing the patch test. *International Journal for Numerical Methods in Engineering*, 26:705–715, 1988.

[28] H. Lamb. On the flexure of an elastic plate. *Proceedings of the London Mathematical Society*, 21:70–91, 1889.

[29] J. Nečas and I. Hlaváček. *Mathematical theory of elastic and elasto-plastic bodies: An introduction*. Elsevier, Amsterdam, Oxford, New York, 1981.

[30] P. Grisvard. *Singularities in boundary value problems*, volume 22 of *Research Notes in Applied Mathematics*. Springer–Verlag, Berlin, Heidelberg, New York, London, 1992.

[31] C. Nazaret. A system of boundary integral equations for polygonal plates with free edges. *Mathematical Methods in the Applied Sciences*, 21:165–185, 1998.

[32] A. Morassi, E. Rosset, and S. Vessella. Detecting general inclusions in elastic plates. *Inverse Problems*, 25(4):045009, 2009.

[33] O. C. Zienkiewicz and R. L. Taylor. *The Finite Element Method*. Butterworth-Heinemann, 2000.

[34] P. G. Bergan. Finite elements based on energy orthogonal functions. *International Journal for Numerical Methods in Engineering*, 15:1541–1555, 1980.

[35] S. Timoshenko and S. Woinowski-Krieger. *Theory of plates and shells*. McGraw–Hill, New York, 2nd edition, 1987.

[36] A. A. Novotny, R. A. Feijóo, C. Padra, and E. Taroco. Topological derivative for linear elastic plate bending problems. *Control and Cybernetics*, 34:339–361, 2005.

[37] V. Sales, A. A. Novotny, and J. E. Muñoz Rivera. Energy change to insertion of inclusions associated with the Reissner–Mindlin plate bending model. *International Journal of Solids and Structures*, 59:132–139, 2015.

Università della Calabria, Dipartimento di Ingegneria Informatica, Modellistica, Elettronica e Sistemistica, via P. Bucci 39/C, 87030 Rende (CS), Italy, www.labmec.unical.it

Email address: antonio.bilotta@unical.it

Università degli Studi di Udine, Dipartimento Politecnico di Ingegneria e Architettura, via Cotonificio 114, 33100 Udine (UD), Italy. Tel.: +39 0432 558739; fax: +39 0432 558700

Email address: antonino.morassi@uniud.it

Università degli Studi di Trieste, Dipartimento di Matematica e Geoscienze, via Valerio 12/1, 34127 Trieste (TS), Italy. Tel.: +39 0432 558739; fax: +39 0432 558700

Email address: rossedi@units.it

Università degli Studi di Sassari, Dipartimento di Architettura, Design e Urbanistica, via Garibaldi 35 - Asilo Sella, 07041 Alghero (SS), Italy

Email address, Corresponding author: emilio.turco@uniss.it

Università degli Studi di Firenze, Dipartimento di Matematica e Informatica "Ulisse Dini", Viale Morgagni, 67/a, 50134 Firenze (FI), Italy

Email address: sergio.vessella@unifi.it